Endogenous hydrogen peroxide positively regulates secretion of a gut-derived peptide in neuroendocrine potentiation of the oxidative stress response in *C. elegans*

Qi Jia[1,3], Drew Young[2,3] and Derek Sieburth[3,4,*]

[1] Development, Stem Cells and Regenerative Medicine PhD program, Keck School of Medicine, University of Southern California, Los Angeles, CA 90033

[2] Neuroscience Graduate Program, University of Southern California, Los Angeles, CA 90089

[3] Zilkha Neurogenetic Institute, University of Southern California, Los Angeles, CA 90033

[4] Department of Physiology and Neuroscience, Keck School of Medicine, University of Southern California, Los Angeles, CA 90033

* Corresponding author
sieburth@med.usc.edu

Keywords: *C. elegans*, oxidative stress, neuropeptide, hydrogen peroxide, mitochondria, superoxide dismutase, peroxiredoxin, thioredoxin, protein kinase C, SNAP25, SOD-1, SOD-3, PRDX-2, TRX-3, PKC-2, AEX-4.

Abstract

The gut-brain axis mediates bidirectional signaling between the intestine and the nervous system and is critical for organism-wide homeostasis. Here we report the identification of a peptidergic endocrine circuit in which bidirectional signaling between neurons and the intestine potentiates the activation of the antioxidant response in *C. elegans.* We identify a FMRF-amide-like peptide, FLP-2, whose release from the intestine is necessary and sufficient to activate the intestinal oxidative stress response by promoting the release of the antioxidant FLP-1 neuropeptide from neurons. FLP-2 secretion from the intestine is positively regulated by endogenous hydrogen peroxide (H_2O_2) produced in the mitochondrial matrix by *sod-3*/superoxide dismutase, and is negatively regulated by *prdx-2*/peroxiredoxin, which depletes H_2O_2 in both the mitochondria and cytosol. H_2O_2 promotes FLP-2 secretion through the DAG and calcium-dependent protein kinase C family member *pkc-2* and by the SNAP25 family member *aex-4* in the intestine. Together, our data demonstrate a role for intestinal H_2O_2 in promoting inter-tissue antioxidant signaling through regulated neuropeptide-like protein exocytosis in a gut-brain axis to activate the oxidative stress response.

Introduction

The gut-brain axis is critical for communication between the intestine and the nervous system to regulate behavior and maintain homeostasis, and altered gut-brain signaling is associated with neurodegeneration, obesity and tumor proliferation (Carabotti et al. 2015; Grenham et al. 2011; Mayer, Nance, and Chen 2022; Mehrian-Shai et al. 2019; Vitali et al. 2022). Over the last decade the importance of peptides that function as signals in gut-brain signaling has gained recognition. Numerous gut peptides are distributed throughout the gastrointestinal (GI) tract with regional specificity (Haber et al. 2017), and gut-secreted peptides can modulate neurocircuits in regulation of feeding behavior and glucose metabolism (Batterham and Bloom 2003; Han et al. 2018; Song et al. 2019), inflammatory responses against pathogenic bacteria (Campos-Salinas et al. 2014; Yu et al. 2021), and satiety (Batterham et al. 2002; Chelikani, Haver, and Reidelberger 2005; Gibbs, Young, and Smith 1973; Lutz et al. 1995; Lutz, Del Prete, and Scharrer 1994; West, Fey, and Woods 1984). A gut-released peptide suppresses arousal through dopaminergic neurons during sleep in *Drosophila* (Titos et al. 2023). In *C. elegans*, gut-derived peptides regulate rhythmic behavior and behavioral responses to pathogenic bacteria (Lee and Mylonakis 2017; Singh and Aballay 2019; Wang et al. 2013). Conversely, peptides released from the nervous system regulate many aspects of intestinal function including gut mobility, inflammation and immune defense (Browning and Travagli 2014; Furness et al. 2014; Lai, Mills, and Chiu 2017). In *C. elegans*, the secretion of peptides from various neurons regulates the mitochondrial unfolded protein response (UPR^{mt}), the heat shock response, and the antioxidant response in the intestine (Jia and Sieburth 2021; Maman et al. 2013; Prahlad, Cornelius, and Morimoto 2008; Shao, Niu, and Liu 2016). In spite of the many roles of peptides in the gut-brain axis, the mechanisms underlying the regulation of intestinal peptide secretion and signaling are not well defined.

Hydrogen peroxide (H_2O_2) is emerging as an important signaling molecule that regulates intracellular signaling pathways by modifying specific reactive residues on target proteins. For example, H_2O_2-regulated phosphorylation of inhibitor of nuclear factor κB (NF-κB) kinase, leads to the activation of NF-κB during development, inflammation and immune responses. (Kamata et al. 2002; Oliveira-Marques et al. 2009; Takada et al. 2003). In addition, H_2O_2 induced tyrosine and cysteine modifications contribute to redox regulation of c-Jun N-terminal kinase 2 (JNK2), Src family kinase, extracellular signal-regulated kinases 1 and 2 (ERK1/2), protein kinase C (PKC) and other protein kinases (Kemble and Sun 2009; Konishi et al. 1997; Lee et al. 2003; Nelson et al. 2018). H_2O_2 signaling has been implicated in regulating neurotransmission and transmitter secretion. H_2O_2 at low concentration increases neurotransmission at neuromuscular junctions without influencing lipid oxidation (Giniatullin and Giniatullin 2003; Giniatullin, Petrov, and Giniatullin 2019; Shakirzyanova et al. 2009). Studies with rat brain tissue demonstrated that enhanced endogenous H_2O_2 generation regulates dopamine release (Avshalumov et al. 2005; Avshalumov and Rice 2003; Bao, Avshalumov, and Rice 2005; Chen, Avshalumov, and Rice 2001, 2002). Acute H_2O_2 treatment increases exocytosis of ATP-containing vesicles in astrocytes (Li et al. 2019). Finally, mitochondrially-derived H_2O_2 regulates neuropeptide release from neurons in *C. elegans* (Jia and Sieburth 2021). Cellular H_2O_2 levels are tightly controlled through the regulation of its production from superoxide by superoxide dismutases (SODs) and cytoplasmic oxidases (Fridovich 1995,

1997; Messner and Imlay 2002; Zelko, Mariani, and Folz 2002), and through its degradation by catalases and peroxidases (Chance, Sies, and Boveris 1979; Marinho et al. 2014). In the intestine, endogenously produced H_2O_2 plays important roles as an antibacterial agent in the lumen, and in activating the ER unfolded protein response (UPR^{ER}) through protein sulfenylation in C. elegans (Botteaux et al. 2009; Corcionivoschi et al. 2012; Hourihan et al. 2016; Miller et al. 2020).

Here we demonstrate a role of endogenous H_2O_2 signaling in the intestine in regulating the release of the intestinal FMRFamide-like peptide, FLP-2, to modulate a neurocircuit that activates the anti-oxidant response in the intestine in *C. elegans.* Intestinal FLP-2 signaling functions by potentiating the release of the antioxidant neuropeptide-like protein FLP-1 from AIY interneurons, which in turn activates the antioxidant response in the intestine. FLP-2 secretion from the intestine is rapidly and positively regulated by H_2O_2. Intestinal H_2O_2 levels and FLP-2 secretion are positively regulated by superoxide dismutases in the mitochondrial matrix and cytosol, and are negatively regulated by the peroxiredoxin-thioredoxin system in the cytosol. Intestinal FLP-2 release is mediated by *aex-4*/SNAP25-dependent exocytosis of dense core vesicles and H_2O_2-induced FLP-2 secretion is dependent upon the production of intestinal diacylglycerol and on *pkc-2*/PKCα/β kinase activity.

Results

Neuronal FLP-1 secretion is regulated by neuropeptide signaling from the intestine.

We previously showed that 10 minute treatment with the mitochondrial toxin juglone leads to a rapid, reversible and specific increase in FLP-1 secretion from AIY, as measured by a two-fold increase in coelomocyte fluorescence in animals expressing FLP-1::Venus fusion proteins in AIY (Fig. 1A and B, (Jia and Sieburth 2021)). Coelomocytes take up secreted neuropeptides by bulk endocytosis (Fares and Greenwald 2001) and the fluorescence intensity of Venus in their endocytic vacuoles is used as a measure of regulated neuropeptide secretion efficacy (Ailion et al. 2014; Ch'ng, Sieburth, and Kaplan 2008; Sieburth, Madison, and Kaplan 2006). To determine the role of the intestine in regulating FLP-1 secretion, we first examined *aex-5* mutants. *aex-5* encodes an intestinal subtilisin/kexin type 5 prohormone convertase (PCSK5), that functions to proteolytically process peptide precursors into mature peptide fragments in dense core vesicles (DCVs) (Edwards et al. 2019; Thacker and Rose 2000), and *aex-5* mutants are defective in peptide signaling from the intestine (Mahoney et al. 2008). We found that *aex-5* mutants expressing FLP-1::Venus in AIY exhibited no significant difference in coelomocyte fluoresce compared to wild type controls in the absence of juglone (Fig. 1B). However, coelomocyte fluorescence did not significantly increase in *aex-5* mutants treated with juglone. Expression of *aex-5* cDNA selectively in the intestine (under the *ges-1* promoter) fully restored normal responses to juglone to *aex-5* mutants, whereas *aex-5* cDNA expression in the nervous system (under the *rab-3* promoter) failed to rescue (Fig. 1B). Thus, peptide processing in intestinal DCVs is necessary for juglone-induced FLP-1 secretion from AIY.

Next, we examined a number of mutants with impaired SNARE-mediated vesicle release in the intestine including *aex-1*/UNC13, *aex*-3/MADD, aex-*4*/SNAP25b, and *aex-6*/Rab27 (Fig. S1A (Iwasaki et al., 1997; Mahoney et al., 2006; Thacker & Rose, 2000; Thomas, 1990; Wang et al., 2013)), and they each exhibited no increases in FLP-1 secretion following juglone treatment above levels observed in untreated controls (Fig. S1B). NLP-40 is a neuropeptide-like protein whose release from the intestine is presumed to be controlled by *aex-1*, *aex-3*, *aex-4* and *aex-6* (Lin-Moore, Oyeyemi, and Hammarlund 2021; Mahoney et al. 2008; Shi et al. 2022; Wang et al. 2013). Null mutants in *nlp-40* or its receptor, *aex-2* (Wang et al. 2013), exhibited normal juglone-induced FLP-1 secretion (Fig. S1C). These results establish a gut-to-neuron signaling pathway that regulates FLP-1 secretion from AIY that is likely to be controlled by peptidergic signaling distinct from NLP-40.

FLP-2 signaling from the intestine potentiates neuronal FLP-1 secretion and the oxidative stress response.

flp-1 protects animals form the toxic effects of juglone (Jia and Sieburth 2021). We reasoned that the intestinal signal that regulates FLP-1 secretion should also protect animals from juglone-induced toxicity. We identified the FMRF-amide neuropeptide-like protein, *flp-2*, in an RNA interference (RNAi) screen for neuropeptides that confer hypersensitivity to juglone toxicity upon knockdown (Jia and Sieburth 2021). *flp-2* signaling has been implicated in regulating lifespan, reproductive development, locomotion during lethargus, and the mitochondrial unfolded protein response (UPR^{mt}) (Chai et al. 2022; Chen et al. 2016; Kageyama et al. 2022; Shao et al. 2016). Putative *flp-2(ok3351)* null mutants, which eliminate most of the *flp-2* coding region, are superficially as healthy as wild type animals, but they exhibited significantly reduced survival in the presence of juglone compared to wild type controls (Fig. 1C). The reduced survival rate of *flp-2* mutants was similar to that of *flp-1* mutants, and *flp-1; flp-2* double mutants exhibited survival rates that were not more severe than those of single mutants (Fig. 1C), suggesting that *flp-1* and *flp-2* may function in a common genetic pathway.

To determine whether *flp-2* signaling regulates FLP-1 secretion from AIY, we examined FLP-1::Venus secretion. *flp-2* mutants exhibited normal levels of FLP-1 secretion in the absence of stress, but FLP-1 secretion failed to significantly increase following juglone treatment of *flp-2* mutants (Fig. 1D). *flp-2* is expressed in a subset of neurons as well as the intestine (Chai et al. 2022), and *flp-2* functions from the nervous system for its roles in development and the UPR^{mt} (Chai et al. 2022; Chen et al. 2016; Kageyama et al. 2022; Shao et al. 2016). Expressing *flp-2* genomic DNA (gDNA) in the nervous system failed to rescue the FLP-1::Venus defects of *flp-2* mutants, whereas expressing *flp-2* selectively in the intestine fully restored juglone-induced FLP-1::Venus secretion to *flp-2* mutants (Fig. 1D). Intestinal overexpression of *flp*-2 had no effect on FLP-1 secretion in the absence of stress, but significantly enhanced the ability of juglone to increase FLP-1 secretion (Fig. 1D). These results indicate that although *flp-2* signaling has minimal impacts on FLP-1 secretion under normal conditions, *flp-2* originating from the intestine is necessary and sufficient to positively regulate FLP-1 release from AIY in the presence of juglone to promote oxidative stress resistance.

198 Previously we showed that FLP-1 signaling from AIY positively regulates the
199 activation of the antioxidant transcription factor SKN-1/Nrf2 in the intestine. Specifically,
200 *flp-1* mutations impair the juglone-induced expression of the SKN-1 reporter transgene
201 P*gst-4::gfp* (Fig. 1E and (Jia and Sieburth 2021)). We found that mutations in *flp-2* caused
202 a similar reduction in juglone-induced P*gst-4::gfp* expression as *flp-1* mutants, and that
203 *flp-1; flp-2* double mutants exhibited similar impairments in juglone-induced P*gst-4::gfp*
204 expression as *flp-1* or *flp-2* single mutants (Fig. 1E). Conversely, overexpression of *flp-2*
205 selectively in the intestine elevated juglone-induced P*gst-4::gfp* expression, without
206 altering baseline P*gst-4::gfp* expression, and the elevated P*gst-4::gfp* expression in
207 juglone-treated animals overexpressing *flp-2* was entirely dependent upon *flp-1* (Fig. 1F).
208 It's noteworthy that overexpressing *flp-2* in the intestine did not enhance FLP-1::Venus
209 release or *Pgst-4::gfp* expression in the absence of stress, indicating that the regulation
210 of the FLP-1 mediated anti-oxidant pathway by *flp-2* is stress activated. Together this data
211 indicates that *flp-2* signaling originating in the intestine positively regulates the stress-
212 induced secretion of FLP-1 from AIY, as well as the subsequent activation of anti-oxidant
213 response genes in the intestine. We propose that FLP-1 and FLP-2 define a bidirectional
214 gut-neuron signaling axis, whereby during periods of oxidative stress, FLP-2 released
215 from the intestine positively regulates FLP-1 secretion from AIY, and FLP-1, in turn,
216 potentiates the antioxidant response in the intestine (Fig. 1A).
217
218 **FLP-2 secretion from the intestine is H_2O_2-regulated.**
219
220 To directly investigate the mechanisms underlying the regulation of FLP-2
221 secretion, we examined FLP-2::Venus fusion proteins expressed in the intestine under
222 various conditions (Fig. 2A). FLP-2::Venus fusion proteins adopted a punctate pattern of
223 fluorescence throughout the cytoplasm of intestinal cells and at the plasma membrane
224 (Fig. 2A), and FLP-2::Venus puncta co-localized with the DCV cargo protein AEX-
225 5/PCSK5 tagged to mTurquoise2 (AEX-5::mTur2, Fig. 2B). FLP-2::Venus fluorescence
226 was also observed in the coelomocytes (marked by mCherry) (Fig. 2A, C), indicating that
227 FLP-2 is released from the intestine. SNAP25 forms a component of the core SNARE
228 complex, which drives vesicular membrane fusion and transmitter release (Chen and
229 Scheller 2001; Goda 1997; Jahn and Scheller 2006). *aex-4* encodes the *C. elegans*
230 homolog of SNAP25, and mutations in *aex-4* disrupt the secretion of neuropeptides from
231 the intestine (Lin-Moore et al. 2021; Mahoney et al. 2008; Wang et al. 2013). We found
232 that *aex-4* null mutations significantly reduced coelomocyte fluorescence in FLP-2::Venus
233 expressing animals, and expression of *aex-4* cDNA selectively in the intestine fully
234 restored FLP-2 secretion to *aex-4* mutants (Fig. 2C). Together these results suggest that
235 intestinal FLP-2 can be packaged into DCVs that undergo release via SNARE-dependent
236 exocytosis.
237 To test whether intestinal FLP-2 secretion is regulated by oxidative stress, we
238 examined coelomocyte fluorescence in FLP-2::Venus-expressing animals that had been
239 exposed to a number of different commonly used oxidative stressors. We found that 10
240 minute exposure to juglone, thimerosal, or paraquat, which promote mitochondria
241 targeted toxicity (Castello, Drechsel, and Patel 2007; Elferink 1999; Sharpe, Livingston,
242 and Baskin 2012), each significantly increased Venus fluorescence intensity in the
243 coelomocytes compared to untreated controls (Fig. 2C and D). We conducted four

controls for specificity: First, juglone treatment did not significantly alter fluorescence intensity of mCherry expressed in coelomocytes (Fig. S2A). Second, impairing intestinal DCV secretion (by either *aex-4*/SNAP25 or *aex-6*/Rab27 mutations (Lin-Moore et al. 2021; Mahoney et al. 2006, 2008; Thomas 1990), blocked the juglone-induced increase in coelomocyte fluorescence in FLP-2::Venus expressing animals (Fig. 2C). Third, *nlp-40* and *nlp-27* encode neuropeptide-like proteins that are released from the intestine (Liu et al. 2023; Taylor et al. 2021; Wang et al. 2013), and juglone treatment had no detectable effects on coelomocyte fluorescence in animals expressing intestinal NLP-40::Venus or NLP-27::Venus fusion proteins (Fig. S2B and C), and NLP-40::mTur2 puncta did not overlap with FLP-2::Venus puncta in the intestine (Fig. S2D). Finally, *flp-1* mutants exhibited wild type levels of FLP-2 secretion both in the absence and presence of juglone (Fig. 2E). The distribution of FLP-2::Venus puncta in the intestine was not detectably altered by juglone treatment. Together, these results indicate that acute oxidative stress selectively increases the exocytosis of FLP-2-containing DCVs from the intestine, upstream of *flp-1* signaling.

SOD-1 and SOD-3 superoxide dismutases regulate FLP-2 release.

Juglone treatment promotes the production of mitochondrial superoxide, which can then be rapidly converted into H_2O_2 by superoxide dismutase. To determine whether H_2O_2 impacts FLP-2 secretion, we first examined superoxide dismutase mutants. *C. elegans* encodes five superoxide dismutase genes (*sod-1* through *sod-5*). *sod-1* or *sod-3* null mutations blocked juglone-induced FLP-2 secretion without altering baseline FLP-2 secretion, whereas *sod-2*, *sod-4*, or *sod-5* mutations had no effect on FLP-2 secretion in the presence of juglone (Fig. 3A and B, S3A). *sod-1; sod-3* double mutants exhibited juglone-induced FLP-2 secretion defects that was similar to single mutants, without significantly altering FLP-2 secretion in the absence of stress (Fig. 3C). *sod-1* encodes the ortholog of mammalian SOD1, which is a cytoplasmic SOD implicated in the development of amyotrophic lateral sclerosis (ALS) and cancer (Giglio et al. 1994; Papa, Manfredi, and Germain 2014; Wang et al. 2021; Zhang et al. 2007). SOD-1::fusion proteins adopted a diffuse pattern of fluorescence in intestinal cells, consistent with a cytoplasmic localization (Fig. 3D). Transgenes expressing the *sod-1* cDNA selectively in the intestine fully rescued the juglone-induced FLP-2::Venus secretion defects of *sod-1* mutants (Fig. 3A). *sod-3* encodes a homolog of mammalian SOD2, which is a mitochondrial matrix SOD implicated in protection against oxidative stress induced neuronal cell death (Fukui and Zhu 2010; Vincent et al. 2007). Intestinal SOD-3::GFP fusion proteins localized to round structures that were surrounded by the outer membrane mitochondrial marker TOMM-20::mCherry (Ahier et al. 2018), consistent with a mitochondrial matrix localization (Fig. 3E). Expression of *sod-3* cDNA in the intestine fully restored juglone induced FLP-2 release to *sod-3* mutants (Fig. 3B). *sod-3* variants lacking the mitochondrial localization sequence (*sod-3*(ΔMLS)), were no longer localized to mitochondria (Fig. 3F) and failed to restore normal responsiveness to juglone to *sod-3* mutants (Fig. 3B). Thus, the generation of H_2O_2 by either SOD-1 in the cytoplasm or by SOD-3 in the mitochondrial matrix is necessary for juglone to increase FLP-2 secretion.

Next, to determine if H_2O_2 can regulate FLP-2 secretion, we examined the effects of acute exogenous H_2O_2 exposure on coelomocyte fluorescence of FLP-2::Venus-

290 expressing animals. We found that 10 minute treatment with H_2O_2 increased FLP-
291 2::Venus secretion to a similar extent as juglone treatment. *aex-4*/SNAP25*,* or *aex-*
292 *6/*Rab27 mutants exhibited no increase in FLP-2 secretion in response to H_2O_2 treatment
293 compared to untreated controls (Fig. 3G). In contrast, *sod-1* or *sod-3* mutants (or *sod-1;*
294 *sod-3* double mutants) exhibited an increase in FLP-2 secretion in response to H_2O_2 that
295 was similar to that of wild type controls (Fig. 3H), suggesting that exogenous H_2O_2 can
296 bypass the requirement of SODs but not SNAREs to promote FLP-2 secretion. Together
297 these results suggest that H_2O_2 generated by SODs can positively regulate intestinal FLP-
298 2 exocytosis form DCVs (Fig. 3I).
299
300 **SOD-1 and SOD-3 regulate intestinal mitochondrial H_2O_2 levels.**
301
302 To directly monitor H_2O_2 levels in the intestine, we generated transgenic animals
303 expressing HyPer7, which is a pH stable genetically encoded H_2O_2 sensor in which the
304 ratio of GFP/CFP fluorescence intensity increases in the presence of H_2O_2 (Pak et al.
305 2020). We targeted HyPer7 to either the mitochondrial matrix (matrix-HyPer7) by
306 generating fusion proteins with the cytochrome c MLS, or to the cytosolic face of the outer
307 mitochondrial membrane (OMM-HyPer7) by generating fusion proteins with TOMM-20.
308 When co-expressed in the intestine with the OMM marker TOMM-20::mCherry, matrix-
309 HyPer7 formed round structures throughout the cytoplasm that were surrounded by the
310 OMM, and OMM-HyPer7 formed ring-like structures throughout the cytoplasm that co-
311 localized with the OMM marker (Fig. 3J). Ten minutes treatment with H_2O_2 significantly
312 increased the fluorescence intensity by about two-fold of both matrix-HyPer7 and OMM-
313 HyPer7 without altering mitochondrial morphology or abundance (Fig. 3J, S3B and C),
314 validating the utility of HyPer7 as a sensor for acute changes in H_2O_2 levels in and around
315 intestinal mitochondria.
316 To determine whether juglone treatment impacts H_2O_2 levels in the intestine, we
317 first treated matrix-HyPer7 expressing animals with juglone for 10 minutes. Juglone
318 treatment led to a similar two-fold increase in matrix-HyPer7 fluorescence as H_2O_2
319 treatment (Fig. 3J). *sod-3* mutations did not alter baseline H_2O_2 levels in the matrix, but
320 they completely blocked juglone-induced increases H_2O_2 levels, whereas *sod-1*
321 mutations had no effect on either baseline or juglone-induced increases H_2O_2 levels (Fig.
322 3J). These results indicate that superoxide produced by juglone treatment is likely to be
323 converted into H_2O_2 by SOD-3 in the matrix (Fig. 3I).
324 Next, we examined H_2O_2 levels on the outer surface of mitochondria using OMM-
325 HyPer7 and we found that juglone treatment led to a two-fold increase in OMM-HyPer7
326 fluorescence, similar to H_2O_2 treatment (Fig. 3J). *sod-3* or *sod-1* mutations did not alter
327 baseline H_2O_2 levels on the OMM, but *sod-1* single mutations attenuated, juglone-induced
328 increases in OMM H_2O_2 levels, while *sod-3* mutations had no effect (Fig. 3J). In *sod-1;*
329 *sod-3* double mutants, the juglone-induced increase in OMM H_2O_2 levels was completely
330 blocked, whereas baseline H_2O_2 levels in the absence of stress were unchanged (Fig.
331 3J). These results suggest that *sod-3* and *sod-1* are exclusively required for H_2O_2
332 production by juglone and that both mitochondrial SOD-3 and cytosolic SOD-1 contribute
333 to H_2O_2 levels in the cytosol. One model that could explain these results is that juglone-
334 generated superoxide is converted into H_2O_2 both by SOD-3 in the matrix, and by SOD-

1 in the cytosol, and that the H_2O_2 generated in the matrix can exit the mitochondria to contribute to cytosolic H_2O_2 levels needed to drive FLP-2 secretion (Fig. 3I).

The peroxiredoxin-thioredoxin system regulates endogenous H_2O_2 levels and FLP-2 secretion.

To determine whether endogenous H_2O_2 regulates FLP-2 secretion, we examined mutations in the peroxiredoxin-thioredoxin system. Peroxiredoxins and thioredoxins detoxify excessive H_2O_2 by converting it into water and they play a critical role in maintaining cellular redox homeostasis (Netto and Antunes 2016) (Fig. 4A). *C. elegans* encodes two peroxiredoxin family members, *prdx-2* and *prdx-3*, that are expressed at high levels in the intestine (Taylor et al. 2021). Null mutations in *prdx-2* significantly increased FLP-2::Venus secretion compared to wild type animals in the absence of stress (Fig. 4B), whereas null mutations in *prdx-3* had no effect on FLP-2 secretion (Fig. S4A). We observed a corresponding increase in both matrix-HyPer7 and OMM-HyPer7 fluorescence intensity in *prdx-2* mutants (Fig. 4C and D), demonstrating that endogenous H_2O_2 is neutralized by peroxiredoxin and establishing a correlation between endogenous H_2O_2 levels and FLP-2 secretion. The increase in FLP-2 secretion in *prdx-2* mutants was not further increased by juglone treatment (Fig. 4B). These results suggest that H_2O_2 generated under either normal conditions or by juglone-treatment can positively regulate FLP-2 secretion.

There are three isoforms of *prdx-2* that arise by the use of alternative transcriptional start sites (Fig. 4A). Expressing the *prdx-2b* isoform selectively in the intestine fully rescued the elevated FLP-2::Venus secretion defects of *prdx-2* mutants, whereas expressing *prdx-2a* or *prdx-2c* isoforms failed to rescue (Fig. 4B, S4B and C). To independently verify the role of *prdx-2b* function in FLP-2 release, we generated a *prdx-2b*-specific knockout mutant by introducing an in frame stop codon within the *prdx-2b*-specific exon 1 using CRISPR/Cas9 (*prdx-2b(vj380)* Fig. 4A). *prdx-2b(vj380)* mutants exhibited increased H_2O_2 levels in the mitochondrial matrix and OMM (Fig. 4C and D), as well as increased FLP-2::Venus secretion compared to wild type controls that were indistinguishable from *prdx-2* null mutants (Fig. 4B). *prdx-2b* mutations could no longer increase FLP-2 secretion when either *sod-1* or *sod-3* activity was impaired (Fig. 4E and Fig. S4D). Thus, the *prdx-2b* isoform normally inhibits FLP-2 secretion likely by promoting the consumption of H_2O_2 in the mitochondrial matrix and/or cytosol.

Once oxidized, peroxiredoxins are reduced by thioredoxins (TRXs) for reuse [refs]. TRX-3 is an intestine-specific thioredoxin promoting protection against specific pathogen infections (Jiménez-Hidalgo et al. 2014; Miranda-Vizuete, Damdimopoulos, and Spyrou 2000; Netto and Antunes 2016). Mutations in *trx-3* elevated FLP-2::Venus release in the absence of juglone and expressing *trx-3* transgenes in the intestine restored wild type FLP-2 release to *trx-3* mutants (Fig. 4B). Juglone treatment failed to further enhance FLP-2::Venus release in *trx-3* mutants (Fig. 4B). Mutations in cytoplasmic *sod-1* but not in mitochondrial *sod-3* reduced the elevated FLP-2::Venus release in *trx-3* mutants to wild type levels (Fig. 4B). Mutations in *trx-3* increased H_2O_2 levels in the OMM but had no effect on matrix H_2O_2 levels (Fig. 4C and D). Thus TRX-3 likely functions in the cytosol but not in the matrix to neutralize H_2O_2, and elevated H_2O_2 levels in the cytosol are sufficient to drive FLP-2 secretion without SOD-3-mediated H_2O_2 generation in the matrix.

381 Finally, to investigate the physiological significance of elevated endogenous H_2O_2
382 levels on the oxidative stress response we examined the effects of *prdx-2b* mutations on
383 expression of *gst-4*. *prdx-2b* mutants had significantly increased P*gst-4::gfp* expression
384 in the intestine compared to wild type controls (Fig. 4F). The increased P*gst-4::gfp*
385 expression in *prdx-2b* mutants was completely dependent upon *flp-2* signaling, since *gst-*
386 *4* expression was reduced to wild type levels in *prdx-2b; flp-2* double mutants (Fig. 4F).
387 Together our data suggest that *prdx-2b* functions in the intestine to maintain redox
388 homeostasis following SOD-1/SOD-3 mediated H_2O_2 production by regulating the
389 secretion of FLP-2 (Fig. 3I).
390
391 **PKC-2/PKCα/β mediates H_2O_2 induced FLP-2 secretion from the intestine.**
392
393 H_2O_2 functions as a cellular signaling molecule by oxidizing reactive cysteines to
394 sulfenic acid, and this modification on target proteins can regulate intracellular signaling
395 pathways (García Santamarina, Boronat i Llop, and Hidalgo Hernando 2014). One of the
396 validated targets of H_2O_2 signaling is the protein kinase C (PKC) family of serine threonine
397 kinases (Jia and Sieburth 2021; Konishi et al. 1997, 2001; Min, Kim, and Exton 1998). *C.*
398 *elegans* encodes four PKC family members including *pkc*-1 and *pkc*-2, which are
399 expressed at highest levels in the intestine (Islas-Trejo et al. 1997; Taylor et al. 2021).
400 *pkc-1* null mutants had no effect on baseline or juglone-induced FLP-2 secretion (Fig.
401 S5A). *pkc-2* null mutations did not alter baseline intestinal FLP-2 secretion, but they
402 eliminated juglone-induced FLP-2 secretion (Fig. 5A). *pkc-2* encodes a calcium and
403 diacylglycerol (DAG) stimulated PKCα/β protein kinase C that regulates thermosensory
404 behavior by promoting transmitter secretion (Edwards et al. 2012; Land and Rubin 2017).
405 Expressing *pkc-2* cDNA selectively in the intestine fully restored juglone-induced FLP-2
406 secretion to *pkc-2* mutants (Fig. 5A), whereas expressing a catalytically inactive *pkc-*
407 *2(K375R)* variant (Van et al. 2021) failed to rescue (Fig. 5A). The intestinal site of action
408 of *pkc-2* is in line with prior studies showing that *pkc-2* can function in the intestine to
409 regulate thermosensory behavior (Land and Rubin 2017). *pkc-2* mutants exhibited wild
410 type H_2O_2 levels in the mitochondrial matrix and OMM of the intestine in both the presence
411 and absence of juglone (Fig. 5B and C). Increasing H_2O_2 levels by either acute H_2O_2
412 treatment or by *prdx-2* mutation failed to increase FLP-2 secretion in *pkc-2* mutants (Fig.
413 5D and E). To determine whether *pkc-2* can regulate the secretion of other peptides from
414 the intestine, we examined expulsion frequency, which is a measure of NLP-40 secretion
415 (Mahoney et al. 2008; Wang et al. 2013). *pkc-2* mutants showed wild type expulsion
416 frequency (Fig. S5B), indicating that intestinal NLP-40 release is largely unaffected.
417 Together, these results show that *pkc-2* is not a general regulator of intestinal peptide
418 secretion, and that PKC-2 functions in the intestine downstream or in parallel to H_2O_2 to
419 promote FLP-2 secretion by a mechanism that involves phosphorylation of target proteins.
420
421 **DAG positively regulates FLP-2 secretion.**
422
423 PKCα/β family members contain two N terminal C1 domains (C1A and C1B) whose
424 binding to DAG promotes PKC recruitment to the plasma membrane (Burns and Bell 1991;
425 Darby, Meng, and Fehrenbacher 2017; Johnson, Giorgione, and Newton 2000; Kim et al.
426 2016; Ono et al. 1989; Yanase et al. 2011). To address the role of DAG in promoting FLP-

427 2 secretion by PKC-2, we examined mutants that are predicted to have altered DAG levels.
428 Phosphatidylinositol phospholipase C beta (PLCβ) converts phosphatidyl inositol
429 phosphate (PIP2) to DAG and inositol triphosphate (IP3, Fig. 6A), and impairing PLC
430 activity leads to reduced cellular DAG levels (Nebigil 1997). *C. elegans* encodes two PLC
431 family members whose expression is enriched in the intestine, *plc-2/* PLCβ and *egl-8/*
432 PLCβ (Taylor et al. 2021). *plc-2* null mutants exhibited baseline and juglone-included FLP-
433 2 secretion that were similar to wild type controls (Fig. S6). *egl-8* loss-of-function mutants
434 exhibited wild type baseline FLP-2 secretion, but juglone-induced FLP-2 secretion was
435 completely blocked (Fig. 6B). H_2O_2 levels in *egl-8* mutants were similar to wild type
436 controls, both in the presence and absence of juglone (Fig. 6C and D). Thus, *egl-8/*PLCβ
437 functions downstream of or in parallel to H_2O_2 production to promote FLP-2 secretion.
438 DAG kinase converts DAG into phosphatidic acid (PA), and is therefore a negative
439 regulator or DAG levels (Fig. 6A) (van Blitterswijk and Houssa 2000; Topham 2006). In
440 *C. elegans*, *dgk-2*/DGKε is the highest expressing DAG kinase in the intestine. Mutations
441 in *dgk-2* elevated FLP-2::Venus secretion (Fig. 6E) without altering H_2O_2 levels in the
442 intestinal mitochondrial matrix or OMM (Fig. 6F and G). Expressing *dgk-2* transgenes
443 selectively in the intestine restored normal FLP-2::Venus secretion to *dgk-2* mutants (Fig.
444 6E). Finally, the increase in FLP-2 secretion in *dgk-2* mutants was not further increased
445 by juglone treatment, but it was completely blocked by *pkc-2* mutations or *aex-4*/SNAP25
446 mutations (Fig. 6E and H). These results show that FLP-2 secretion can be regulated
447 bidirectionally by DAG, and they suggest that DAG and H_2O_2 function in a common
448 genetic pathway upstream of *pkc-2* to promote FLP-2 secretion (Fig. 6A).
449
450
451 **Discussion**
452
453 By screening for intercellular regulators of FLP-1 signaling from the nervous
454 system in promoting the anti-oxidant response, we have uncovered a function for
455 peptidergic signaling in mediating gut-to-neuron regulation of the anti-oxidant response
456 in *C. elegans.* We identified the neuropeptide-like protein FLP-2 as an inter-tissue signal
457 originating in the intestine to potentiate stress-induced FLP-1 release from AIY neurons
458 and the subsequent activation of SKN-1 in the intestine. We found that H_2O_2 generated
459 endogenously in the intestine or exogenously by acute oxidant exposure increases FLP-
460 2 secretion from intestinal DCVs. H_2O_2 promotes FLP-2 exocytosis through PKC-2, and
461 AEX-4/SNAP25. The use of oxidant-regulated peptide secretion exemplifies a
462 mechanism that can allow the gut and the nervous system to efficiently and rapidly
463 communicate through endocrine signaling to promote organism-wide protection in the
464 face of intestinal stress (Fig. 6I).
465
466 **A new function for *flp-2* signaling in the antioxidant response.**
467
468 Previous studies have identified roles for *flp-2* signaling in development and in
469 stress responses. *flp-2* promotes locomotion during molting (Chen et al. 2016) promotes
470 entry into reproductive growth (Chai et al. 2022), regulates longevity (Kageyama et al.
471 2022), and activates the UPR^{mt} cell-non autonomously during mitochondrial stress (Shao
472 et al. 2016). The function we identified for *flp-2* in the antioxidant response has some

473 notable similarities with *flp-2*'s other functions. First, *flp-2* mediates its effects at least in
474 part by regulating signaling by other peptides. *flp-2* signaling increases the secretion of
475 the neuropeptide like protein PDF-1 during lethargus (Chen et al. 2016) and INS-
476 35/insulin-like peptide for its roles in reproductive growth choice and longevity (Kageyama
477 et al. 2022), in addition to regulating AIY FLP-1 secretion (Fig. 5G). In mammals, release
478 of the RF-amide neuropeptide kisspeptin from the anteroventral periventricular nucleus
479 (AVPV) regulates reproduction by inducing the release of gonadotropins via its stimulatory
480 action on GnRH neurons (Han et al. 2005). Second, the secretion of FLP-2 is dynamic.
481 FLP-2 secretion decreases during lethargus (Chen et al. 2016) and increases under
482 conditions that do not favor reproductive growth (Kageyama et al. 2022), as well
483 increasing in response to oxidants (Fig. 2C and D). However, in some instances, the
484 regulation of FLP-2 secretion may occur at the level of flp-2 expression (Kageyama et al.
485 2022), rather than at the level of exocytosis (Fig. 2C). Finally, genetic analysis of *flp-2* has
486 revealed that under normal conditions, *flp-2* signaling may be relatively low, since *flp-2*
487 mutants show no defects in reproductive growth choice when animals are well fed (Chai
488 et al. 2022), show only mild defects in locomotion during molting in non-sensitized genetic
489 backgrounds (Chen et al. 2016), and do not have altered baseline FLP-1 secretion or
490 antioxidant gene expression in the absence of exogenous oxidants (Fig. 1D and E). It is
491 notable that increased ROS levels are associated with molting (Back et al. 2012; Knoefler
492 et al. 2012), ageing (Back et al. 2012; Van Raamsdonk and Hekimi 2010), starvation (Tao
493 et al. 2017), and mitochondrial dysfunction (Dingley et al. 2010), raising the possibility
494 that *flp-2* may be used in specific contexts associated with high ROS levels to affect global
495 changes in physiology, behavior and development.
496 One major difference we found for *flp-2* signaling in our study is that intestinal, but
497 not neuronal *flp-2* activates the oxidative stress response, whereas *flp-2* originates from
498 neurons for its reported roles in development and the UPR^{mt}. The intestine is uniquely
499 poised to relay information about diet to the rest of the animal, and secretion of a number
500 of neuropeptide-like proteins from the intestine (e.g, INS-11, PDF-2 and INS-7) is
501 proposed to regulate responses to different bacterial food sources (Lee and Mylonakis
502 2017; Murphy, Lee, and Kenyon 2007; O'Donnell et al. 2018). Since bacterial diet can
503 impact ROS levels in the intestine (Pang and Curran 2014), secretion of FLP-2 from the
504 intestine could function to relay information about bacterial diet to distal tissues to regulate
505 redox homeostasis. In addition, the regulation of intestinal FLP-2 release by oxidants may
506 meet a unique spatial, temporal or concentration requirement for activating the antioxidant
507 response that cannot be met by its release from the nervous system.
508
509 **AIY as a target for *flp-2* signaling.**
510
511 AIY interneurons receive sensory information from several neurons primarily as
512 glutamatergic inputs to regulate behavior (Bargmann et al. 2007; Clark et al. 2006; Satoh
513 et al. 2014). Our study reveals a previously undescribed mechanism by which AIY is
514 activated through endocrine signaling originating from FLP-2 secretion from the intestine.
515 FLP-2 could act directly on AIY, or it may function indirectly through upstream neurons
516 that relay FLP-2 signals to AIY. *frpr-18* encodes an orexin-like GPCR that can be activated
517 by FLP-2-derived peptides in transfected mammalian cells (Larsen et al. 2013; Mertens
518 et al. 2005), and *frpr-18* functions downstream of *flp-2* in the locomotion arousal circuit

(Chen et al. 2016). *frpr-18* is expressed broadly in the nervous system including in AIY (Chen et al. 2016), and loss-of-function *frpr-18* mutations lead to hypersensitivity to certain oxidants (Ouaakki et al. 2023). FRPR-18 is coupled to the heterotrimeric G protein Gαq (Larsen et al. 2013; Mertens et al. 2005), raising the possibility that FLP-2 may promote FLP-1 secretion from AIY by directly activating FRPR-18 in AIY. However, *flp-2* functions independently of *frpr-18* in the reproductive growth circuit, and instead functions in a genetic pathway with the GPCR *npr-30* (Chai et al. 2022). In addition, FLP-2-derived peptides can bind to the GPCRs DMSR-1, or DMSR-18 in transfected cells (Beets et al. 2023). Identifying the FLP-2 receptor and its site of action will help to define the circuit used by intestinal *flp-2* to promote FLP-1 release from AIY.

FLP-1 release from AIY is positively regulated by H_2O_2 levels generated from mitochondria (Jia and Sieburth 2021). Here we showed that FLP-1 release is also regulated by intestinal FLP-2 signaling. Interestingly, H_2O_2 treatment is not sufficient to promote FLP-1 secretion in the absence of *flp-2*, and intestinal-derived FLP-2 is not sufficient to promote FLP-1 secretion in the absence of H_2O_2 (Fig. 1D). These results point to a model whereby AIY must integrate at least two stress signals: increased mt H_2O_2 levels and increased *flp-2* signaling input, and only when both conditions are met will FLP-1 secretion increase. AIY shows a sporadic Ca^{2+} response regardless of the presence of explicit stimulation (Ashida, Hotta, and Oka 2019; Bargmann et al. 2007; Clark et al. 2006), and FLP-1 secretion from AIY is calcium dependent (Jia and Sieburth 2021). How mitochondrial H_2O_2 levels are established in AIY by intrinsic or extracellular inputs, and how AIY integrates H_2O_2 and *flp-2* signaling to control FLP-1 secretion remain to be defined.

A role for endogenous H_2O_2 in regulated neuropeptide secretion.

Using HyPer7, we showed that acute juglone exposure results in a rapid elevation of endogenous H_2O_2 levels inside and outside intestinal mitochondria and a corresponding increase of FLP-2 release from the intestine that depends on the cytoplasmic superoxide dismutase *sod-1*, and mitochondrial *sod-3*. We favor a model whereby superoxide generated by juglone in the mitochondria is converted to H_2O_2 by SOD-3 in the matrix and by SOD-1 in the cytosol. In this case, both the superoxide generated by juglone and the H_2O_2 generated by SOD-3 would have to be able to exit the mitochondria and enter the cytosol. Superoxide and H_2O_2 can be transported across mitochondrial membranes through anion channels and aquaporin channels, respectively (Bienert and Chaumont 2014; Ferri et al. 2003; Han et al. 2003; Kontos et al. 1985). The observation that both SOD-1 and SOD-3 activity are necessary to drive FLP-2 release suggests that H_2O_2 levels much reach a certain threshold in the cytoplasm to promote FLP-2 release, and this threshold requires the generation of H_2O_2 by both SOD-1 and SOD-3.

We identified a role for the antioxidant peroxiredoxin-thioredoxin system, encoded by *prdx-2* and *trx-3*, in maintaining low endogenous H_2O_2 levels in the intestine and in negatively regulating FLP-2 secretion. We showed that the *prdx-2b* isoform functions to inhibit FLP-2 secretion and to lower H_2O_2 levels in both the mitochondrial matrix and on the cytosolic side of mitochondria. These observations are consistent with a subcellular site of action for PRDX-2B in either the matrix only or in both the matrix and cytosol. In

565 contrast, *trx-3* mutations do not alter mitochondrial H_2O_2 levels, suggesting that TRX-3
566 functions exclusively in the cytosol. Thus, the PRDX-2B-TRX-3 combination may function
567 in the cytosol, and PRDX-2B may function with a different TRX family member in the
568 matrix. There are several thioredoxin-domain containing proteins in addition to *trx-3* in the
569 *C. elegans* genome that could be candidates for this role. Alternatively, *prdx-2* may
570 function alone or with other redox proteins. PRDX-2 may function without thioredoxins in
571 its roles in light sensing and stress response in worms (Li et al. 2016; Oláhová et al. 2008;
572 Oláhová and Veal 2015). PRDX-2B contains a unique N terminal domain that is distinct
573 from the catalytic domain and is not found on the other PRDX-2 isoforms. This domain
574 may be important for targeting PRDX-2B to specific subcellular location(s) where it can
575 regulate FLP-2 secretion.
576
577 **Regulation of FLP-2 exocytosis by PKC-2/PKCα/β and AEX-4/SNAP25.**
578
579 We demonstrated that *pkc-2* mediates the effects of H_2O_2 on intestinal FLP-2
580 secretion, and H_2O_2- and DAG-mediated PKC-2 activation are likely to function in a
581 common genetic pathway to promote FLP-2 secretion. Our observations that DAG is
582 required for the effects of juglone (Fig. 6B), are consistent with a two-step activation model
583 for PKC-2, in which H_2O_2 could first modify PKC-2 in the cytosol, facilitating subsequent
584 PKC-2 recruitment to the membrane by DAG. Alternatively, DAG could first recruit PKC-
585 2 to membranes, where it is then modified by H_2O_2. We favor a model whereby H_2O_2
586 modification occurs in the cytosol, since H_2O_2 produced locally by mitochondria would
587 have access to cytosolic pools of PKC-2 prior to its membrane translocation.
588 We defined a role for *aex-4*/SNAP25 in the fusion step of FLP-2 containing DCVs
589 from the intestine under normal conditions as well as during oxidative stress. In
590 neuroendocrine cells, phosphorylation of SNAP25 on Ser187 potentiates DCV
591 recruitment into releasable pools (Nagy et al. 2002; Shu et al. 2008; Yang et al. 2007),
592 and exocytosis stimulated by the DAG analog phorbol ester (Gao et al. 2016; Shu et al.
593 2008), without altering baseline SNAP25 function. Interestingly, the residue
594 corresponding to Ser187 is conserved in AEX-4, raising the possibility that PKC-2
595 potentiates FLP-2 secretion by phosphorylating AEX-4. Since SNAP25 phosphorylation
596 on Ser187 has been shown to increase its interaction with syntaxin and promote SNARE
597 complex assembly in vitro (Gao et al. 2016; Yang et al. 2007), it is possible that elevated
598 H_2O_2 levels could promote FLP-2 secretion by positively regulating SNARE-mediated
599 DCV fusion at intestinal release sites on the basolateral membrane through AEX-
600 4/SNAP25 phosphorylation by PKC-2. Prior studies have shown that PKC-2
601 phosphorylates the SNARE-associated protein UNC-18 in neurons to regulate
602 thermosensory behavior (Edwards et al. 2012; Land and Rubin 2017). Thus, PKC-2 may
603 have multiple targets in vivo and target selection may be dictated by cell type and/or the
604 redox status of the cell.
605
606 **Similar molecular mechanisms regulating FLP-1 and FLP-2 release.**
607
608 The molecular mechanisms we identified that regulate FLP-2 secretion from the
609 intestine are similar in several respects to those regulating FLP-1 secretion from AIY. First,
610 the secretion of both peptides is positively regulated by H_2O_2 originating from

611 mitochondria. Second, in both cases, H_2O_2 promotes exocytosis of neuropeptide-
612 containing DCVs by a mechanism that depend upon the kinase activity of protein kinase
613 C. Finally, the secretion of both peptides is controlled through the regulation of H_2O_2 levels
614 by superoxide dismutases and by the peroxiredoxin-thioredoxin system. H_2O_2-regulated
615 FLP-1 and FLP-2 secretion differ in the identity of the family members of some of the
616 genes involved. *prdx-3-trx-2* and *sod-2* family members regulate H_2O_2 levels in AIY,
617 whereas *prdx-2-trx-3* and *sod-1/sod-3* family members regulate H_2O_2 levels in the
618 intestine. In addition, *pkc-1* promotes H_2O_2 induced FLP-1 secretion from AIY whereas
619 *pkc-2* promotes H_2O_2 -induced FLP-2 secretion from the intestine. Nonetheless, it is
620 noteworthy that two different cell types utilize largely similar pathways for the H_2O_2-
621 mediated regulation of neuropeptide release, raising the possibility that similar
622 mechanisms may be utilized in other cell types and/or organisms to regulate DCV
623 secretion.
624
625
626 **Materials and Methods**
627
628 **Strains and transgenic lines**
629 *C. elegans* strains were maintained at 20°C in the dark on standard nematode
630 growth medium (NGM) plates seeded with OP50 Escherichia coli as food source, unless
631 otherwise indicated. All strains were synchronized by picking mid L4 stage animal either
632 immediately before treatment (for coelomocyte imaging and intestine imaging) or 24h
633 before treatment (for P*gst-4::gfp* imaging). The wild type strain was Bristol N2. Mutants
634 used in this study were out-crossed at least four times.
635 Transgenic lines were generated by microinjecting plasmid mixes into the gonads
636 of young adult animals following standard techniques (Mello et al. 1991). Microinjection
637 mixes were prepared by mixing expression constructs with the co-injection markers
638 pJQ70 (P*ofm-1::rfp*, 25ng/μL), pMH163 (P*odr-1::mCherry*, 40ng/μL), pMH164 (P*odr-*
639 *1::gfp*, 40ng/μL) or pDS806 (P*myo-3::mCherry*, 20ng/μL) to a final concentration of
640 100ng/μL. For tissue-specific expression, a 1.5kb *rab-3* promoter was used for pan-
641 neuronal expression (Nonet et al. 1997), a 2.0kb *ges-1* or a 3.5kb *nlp-40* promoter was
642 used for intestinal expression (Egan et al. 1995; Wang et al. 2013). At least three
643 transgenic lines were examined for each transgene, and one representative line was used
644 for quantification. Strains and transgenic lines used in this study are listed in the
645 Supplementary Table.
646
647 **Molecular Biology**
648 All gene expression vectors were constructed with the backbone of pPD49.26.
649 Promoter fragments including P*rab-3*, and P*ges-1* were amplified from genomic DNA;
650 genes of interest, including cDNA fragments (*aex-5, snt-5, sod-1b, sod-3, isp-1, prdx-2a,*
651 *prdx-2b, prdx-2c, trx-3, pkc-2b, dgk-2a, aex-4*) and genomic fragments (*flp-2, flp-40, nlp-*
652 *36, nlp-27*) were amplified from cDNA library and genomic DNA respectively using
653 standard molecular biology protocols. Expression plasmid of HyPer7 was designed based
654 on reported mammalian expression plasmid for HyPer7 (Pak et al. 2020) and was
655 synthesized by Thermo Fisher Scientific with codon optimization for gene expression in
656 *C. elegans.* Plasmids and primers used in this study are listed in the Supplementary Table.

657
658 **Toxicity Assay**
659 Stock solution of 50mM juglone in DMSO was freshly made on the same day of
660 liquid toxicity assay, working solution of juglone in M9 buffer was prepared using stock
661 solution before treatment. Around 60-80 synchronized adult animals were transferred into
662 a 1.5mL Eppendorf tube with fresh M9 buffer and washed three times. Working solution
663 of juglone was added to the animals at indicated concentration. Animals were incubated
664 in dark for 4h on rotating mixer before being transferred onto fresh NGM plates seeded
665 with OP50 to recover in dark at 20°C. Percentage of survival was assayed by counting
666 the number of alive and dead animals. Toxicity assays were performed in triplicates.
667
668 **RNAi Interference**
669 Plates for feeding RNAi interference were prepare as described (Kamath 2003).
670 Around 20-25 gravid adult animals with indicated genotype were transferred onto the
671 RNAi plates that were seeded with HT115(DE3) bacteria transformed with L4440 vectors
672 with targeted gene inserts or empty L4440 vectors. Eggs were collected for 4h to obtain
673 synchronized populations. L4 stage animals were collected for further assays. RNAi
674 clones were from Ahringer or Vidal RNAi library, or made from genomic DNA. Details were
675 listed in the Supplementary Table.
676
677 **Behavioral assays**
678 The defecation motor program was assayed as previously described (Liu and
679 Thomas 1994). Twenty to thirty L4 animals were transferred onto a fresh NGM plate
680 seeded with OP50 *E. coli* and were stored in a 20°C incubator for 24 hours. After 24 hours,
681 ten consecutive defecation cycles were observed from three independent animals and
682 the mean and the standard error was calculated for each genotype. The pBoc and aBoc
683 steps were recorded using custom Etho software (James Thomas Lab
684 website:http://depts.washington.edu/jtlab/software/otherSoftware.html)
685
686 **Microscopy and Fluorescence Imaging**
687 Approximately 30-40 age matched animals were paralyzed with 30mg/mL 2,3-
688 butanedione monoxime (BDM) in M9 buffer and mounted on 2% agarose pads. Images
689 were captured using the Nikon eclipse 90i microscope equipped with Nikon Plan Apo 20x,
690 40x, 60x, and 100x oil objective (N.A.=1.40), and a Photometrics Coolsnap ES2 camera
691 or a Hamamatsu Orca Flash LT+CMOS camera. Metamorph 7.0 software (Universal
692 Imaging/Molecular Devices) was used to capture serial image stacks and to obtain the
693 maximum intensity projection image for analysis.
694 For transcriptional reporter imaging, young adult animals with indicated genotype
695 were transferred into a 1.5mL Eppendorf tube with M9 buffer, washed three times and
696 incubated in working solution of juglone with indicated concentration for 4h in dark on
697 rotating mixer before recovering on fresh NGM plates with OP50 for 1h in dark at 20°C.
698 The posterior end of the intestine was imaged with the 60x objective and quantification
699 for average fluorescence intensity of a 16-pixel diameter circle in the posterior intestine
700 was calculated using Metamorph.
701 For coelomocyte imaging, L4 stage animals were transferred in fresh M9 buffer on
702 a cover slide, washed six times with M9 before being exposed to juglone or H_2O_2 in M9

buffer. Animals were then paralyzed in BDM and images of coelomocytes next to the posterior end of intestine were taken using the 100x oil objective. Average fluorescence intensity of Venus from the endocytic compartments in the posterior coelomocytes was measured in ImageJ.

For fusion protein fluorescence imaging, L4 stage animals were exposed to M9 buffer or indicated oxidants for 10min before being paralyzed in BDM and taken images of the posterior end of the intestine using 100x oil objective. For HyPer7 imaging, Z stacks were obtained using GFP (excitation/emission: 500nm/520nm) and CFP (excitation/emission: 400nm/520nm) filter sets sequentially, HyPer7 fluorescence signal was quantified as the ratio of GFP to CFP fluorescence intensity changes with respect to the baseline [(Ft − F0)/F0].

CRISPR/Cas9 Editing

prdx-2b(vj380) knock-out mutants were generated using a co-CRISPR protocol (Arribere et al. 2014). A sgRNA and a repair single stranded oligodeoxynucleotides (ssODN) targeting *dpy-10* were co-injected with a sgRNA for genes of interest and a ssODN that induces homology-directed repaire (HDR) to introduce Cas9 mediated mutagenesis. Fifteen young adult animals were injected to produce around thirty singled F1 animals carrying Dpy or Rol phenotype. F2 animals were genotyped for mutations based on PCR and enzyme digest. Homozygous mutants were outcrossed with wild type animals at least four times before being used for assays.

Statistics

Statistical analysis was performed on GraphPad Prism 9. Unpaired *t*-test with two tails was used for two groups and one-way ANOVA with multiple comparison corrections was used to three or more groups to determine the statistical significance. Statistical details and n are specified in the figure legends. All comparisons are conducted based on wild-type controls unless indicated by lines between genotypes. Bar graphs with plots were generated using GraphPad Prism 9.

Acknowledgement

C. elegans strains used in this study were provided by the Caenorhabditis Genetics Centre (CGC), which is funded by the NIH National Center for Research Resources (NCRR). We thank members of the Sieburth lab for critical reading and discussion of the manuscript. This work was supported by grants from National Institute of Health NINDS R01NS071085 and R01NS110730 to D.S.

Reference

Ahier, Arnaud, Chuan-Yang Dai, Andrea Tweedie, Ayenachew Bezawork-Geleta, Ina Kirmes, and Steven Zuryn. 2018. “Affinity Purification of Cell-Specific Mitochondria from Whole Animals Resolves Patterns of Genetic Mosaicism.” *Nature Cell Biology* 20(3):352-. doi: 10.1038/s41556-017-0023-x.

Ailion, Michael, Mandy Hannemann, Susan Dalton, Andrea Pappas, Shigeki Watanabe, Jan Hegermann, Qiang Liu, Hsiao-Fen Han, Mingyu Gu, Morgan Q. Goulding, Nikhil Sasidharan, Kim Schuske, Patrick Hullett, Stefan Eimer, and Erik M. Jorgensen. 2014. “Two Rab2 Interactors Regulate Dense-Core Vesicle Maturation.” *Neuron* 82(1):167–80. doi: 10.1016/j.neuron.2014.02.017.

Arribere, Joshua A., Ryan T. Bell, Becky XH Fu, Karen L. Artiles, Phil S. Hartman, and Andrew Z. Fire. 2014. “Efficient Marker-Free Recovery of Custom Genetic Modifications with CRISPR/Cas9 in Caenorhabditis Elegans.”

Ashida, Keita, Kohji Hotta, and Kotaro Oka. 2019. “The Input-Output Relationship of AIY Interneurons in Caenorhabditis Elegans in Noisy Environment.” *iScience* 19:191–203. doi: 10.1016/j.isci.2019.07.028.

Avshalumov, Marat V., Billy T. Chen, Tibor Koos, James M. Tepper, and Margaret E. Rice. 2005. “Endogenous Hydrogen Peroxide Regulates the Excitability of Midbrain Dopamine Neurons via ATP-Sensitive Potassium Channels.” *The Journal of Neuroscience* 25(17):4222–31. doi: 10.1523/JNEUROSCI.4701-04.2005.

Avshalumov, Marat V., and Margaret E. Rice. 2003. “Activation of ATP-Sensitive K+ (KATP) Channels by H2O2 Underlies Glutamate-Dependent Inhibition of Striatal Dopamine Release.” *Proceedings of the National Academy of Sciences - PNAS* 100(20):11729–34. doi: 10.1073/pnas.1834314100.

Back, Patricia, Winnok H. De Vos, Geert G. Depuydt, Filip Matthijssens, Jacques R. Vanfleteren, and Bart P. Braeckman. 2012. “Exploring Real-Time in Vivo Redox Biology of Developing and Aging Caenorhabditis Elegans.” *Free Radical Biology & Medicine* 52(5):850–59. doi: 10.1016/j.freeradbiomed.2011.11.037.

Bao, Li, Marat V. Avshalumov, and Margaret E. Rice. 2005. “Partial Mitochondrial Inhibition Causes Striatal Dopamine Release Suppression and Medium Spiny Neuron Depolarization via H2O2 Elevation, Not ATP Depletion.” *The Journal of Neuroscience* 25(43):10029–40. doi: 10.1523/JNEUROSCI.2652-05.2005.

Bargmann, Cornelia I., Sreekanth H. Chalasani, Nikos Chronis, Makoto Tsunozaki, Jesse M. Gray, Daniel Ramot, and Miriam B. Goodman. 2007. “Dissecting a Circuit for Olfactory Behaviour in Caenorhabditis Elegans.” *Nature* 450(7166):63–70. doi: 10.1038/nature06292.

Batterham, Rachel L., and Stephen R. Bloom. 2003. “The Gut Hormone Peptide YY Regulates Appetite.” *Annals of the New York Academy of Sciences* 994(1):162–68. doi: 10.1111/j.1749-6632.2003.tb03176.x.

Batterham, Rachel L., Michael A. Cowley, Caroline J. Small, Herbert Herzog, Mark A. Cohen, Catherine L. Dakin, Alison M. Wren, Audrey E. Brynes, Malcolm J. Low, Mohammad A. Ghatei, Roger D. Cone, and Stephen R. Bloom. 2002. “Gut Hormone PYY(3-36) Physiologically Inhibits Food Intake.” *Nature (London)* 418(6898):650-.

Beets, Isabel, Sven Zels, Elke Vandewyer, Jonas Demeulemeester, Jelle Caers, Esra Baytemur, Amy Courtney, Luca Golinelli, İlayda Hasakioğulları, William R. Schafer, Petra E. Vértes, Olivier Mirabeau, and Liliane Schoofs. 2023. “System-Wide Mapping of Peptide-GPCR Interactions in C. Elegans.” *Cell Reports (Cambridge)* 42(9):113058–113058. doi: 10.1016/j.celrep.2023.113058.

Bienert, Gerd P., and François Chaumont. 2014. “Aquaporin-Facilitated Transmembrane Diffusion of Hydrogen Peroxide.” *Biochimica et Biophysica Acta* 1840(5):1596–1604. doi: 10.1016/j.bbagen.2013.09.017.

van Blitterswijk, Wim J., and Brahim Houssa. 2000. “Properties and Functions of Diacylglycerol Kinases.” *Cellular Signalling* 12(9):595–605. doi: 10.1016/S0898-6568(00)00113-3.

Botteaux, A., C. Hoste, J. E. Dumont, J. Van Sande, and A. Allaoui. 2009. “Potential Role of Noxes in the Protection of Mucosae: H(2)O(2) as a Bacterial Repellent.” *Microbes and Infection* 11(5):537–44. doi: 10.1016/j.micinf.2009.02.009.

Browning, Kirsteen N., and R. Alberto Travagli. 2014. “Central Nervous System Control of Gastrointestinal Motility and Secretion and Modulation of Gastrointestinal Functions.” *Comprehensive Physiology* 4(4):1339–68. doi: 10.1002/cphy.c130055.

Burns, D. J., and R. M. Bell. 1991. “Protein Kinase C Contains Two Phorbol Ester Binding Domains.” *The Journal of Biological Chemistry* 266(27):18330–38. doi: 10.1016/S0021-9258(18)55274-1.

Campos-Salinas, Jenny, Antonio Cavazzuti, Francisco O'Valle, Irene Forte-Lago, Marta Caro, Stephen M. Beverley, Mario Delgado, and Elena Gonzalez-Rey. 2014. "Therapeutic Efficacy of Stable Analogues of Vasoactive Intestinal Peptide against Pathogens." *The Journal of Biological Chemistry* 289(21):14583–99. doi: 10.1074/jbc.M114.560573.

Carabotti, Marilia, Annunziata Scirocco, Maria Antonietta Maselli, and Carola Severi. 2015. "The Gut-Brain Axis: Interactions between Enteric Microbiota, Central and Enteric Nervous Systems." *Annals of Gastroenterology* 28(2):203–9.

Castello, Pablo R., Derek A. Drechsel, and Manisha Patel. 2007. "Mitochondria Are a Major Source of Paraquat-Induced Reactive Oxygen Species Production in the Brain." *The Journal of Biological Chemistry* 282(19):14186–93. doi: 10.1074/jbc.M700827200.

Chai, Cynthia M., Mahdi Torkashvand, Maedeh Seyedolmohadesin, Heenam Park, Vivek Venkatachalam, and Paul W. Sternberg. 2022. "Interneuron Control of C. Elegans Developmental Decision-Making." *Current Biology* 32(10):2316-2324.e4. doi: 10.1016/j.cub.2022.03.077.

Chance, B., H. Sies, and A. Boveris. 1979. "Hydroperoxide Metabolism in Mammalian Organs." *Physiological Reviews* 59(3):527–605. doi: 10.1152/physrev.1979.59.3.527.

Chelikani, Prasanth K., Alvin C. Haver, and Roger D. Reidelberger. 2005. "Intravenous Infusion of Peptide YY(3–36) Potently Inhibits Food Intake in Rats." *Endocrinology (Philadelphia)* 146(2):879–88. doi: 10.1210/en.2004-1138.

Chen, Billy T., Marat V. Avshalumov, and Margaret E. Rice. 2001. "H2O2 Is a Novel, Endogenous Modulator of Synaptic Dopamine Release." *Journal of Neurophysiology* 85(6):2468–76. doi: 10.1152/jn.2001.85.6.2468.

Chen, Billy T., Marat V. Avshalumov, and Margaret E. Rice. 2002. "Modulation of Somatodendritic Dopamine Release by Endogenous H2O2: Susceptibility in Substantia Nigra But Resistance in VTA." *Journal of Neurophysiology* 87(2):1155–58. doi: 10.1152/jn.00629.2001.

Chen, Didi, Kelsey P. Taylor, Qi Hall, and Joshua M. Kaplan. 2016. "The Neuropeptides FLP-2 and PDF-1 Act in Concert To Arouse Caenorhabditis Elegans Locomotion." *Genetics (Austin)* 204(3):1151–59. doi: 10.1534/genetics.116.192898.

Chen, Yu A., and Richard H. Scheller. 2001. "SNARE-Mediated Membrane Fusion." *Nature Reviews. Molecular Cell Biology* 2(2):98–106. doi: 10.1038/35052017.

Ch'ng, Queelim, Derek Sieburth, and Joshua M. Kaplan. 2008. "Profiling Synaptic Proteins Identifies Regulators of Insulin Secretion and Lifespan." *PLoS Genetics* 4(11):e1000283. doi: 10.1371/journal.pgen.1000283.

Clark, Damon A., David Biron, Piali Sengupta, and Aravinthan D. T. Samuel. 2006. "The AFD Sensory Neurons Encode Multiple Functions Underlying Thermotactic Behavior in Caenorhabditis Elegans." *The Journal of Neuroscience* 26(28):7444–51. doi: 10.1523/JNEUROSCI.1137-06.2006.

Corcionivoschi, Nicolae, Luis AJ Alvarez, Thomas H. Sharp, Monika Strengert, Abofu Alemka, Judith Mantell, Paul Verkade, Ulla G. Knaus, and Billy Bourke. 2012. "Mucosal Reactive Oxygen Species Decrease Virulence by Disrupting Campylobacter Jejuni Phosphotyrosine Signaling." *Cell Host & Microbe* 12(1):47–59. doi: 10.1016/j.chom.2012.05.018.

Darby, Lisa M., Hongdi Meng, and Jill C. Fehrenbacher. 2017. "Paclitaxel Inhibits the Activity and Membrane Localization of PKCα and PKCβI/II to Elicit a Decrease in Stimulated Calcitonin Gene-Related Peptide Release from Cultured Sensory Neurons." *Molecular and Cellular Neurosciences* 82:105–17. doi: 10.1016/j.mcn.2017.04.001.

Dingley, Stephen, Erzsebet Polyak, Richard Lightfoot, Julian Ostrovsky, Meera Rao, Todd Greco, Harry Ischiropoulos, and Marni J. Falk. 2010. "Mitochondrial Respiratory Chain Dysfunction Variably Increases Oxidant Stress in Caenorhabditis Elegans." *Mitochondrion* 10(2):125–36. doi: 10.1016/j.mito.2009.11.003.

Edwards, Mark R., James R. Johnson, Kimberley Rankin, Rosalind E. Jenkins, Carl Maguire, Alan Morgan, Robert D. Burgoyne, and Jeff W. Barclay. 2012. "PKC-2 Phosphorylation of UNC-18 Ser322 in AFD Neurons Regulates Temperature Dependency of Locomotion." *The Journal of Neuroscience* 32(20):7042–51. doi: 10.1523/JNEUROSCI.4029-11.2012.

Edwards, Samantha Louise, Lucas Mergan, Bhavesh Parmar, Bram Cockx, Wouter De Haes, Liesbet Temmerman, and Liliane Schoofs. 2019. "Exploring Neuropeptide Signalling through Proteomics and Peptidomics." *Expert Review of Proteomics* 16(2):131–37. doi: 10.1080/14789450.2019.1559733.

Egan, Cay R., May A. Chung, Fran L. Allen, Mark FP Heschl, Cheryl L. Van Buskirk, and James D. McGhee. 1995. "A Gut-to-Pharynx/Tail Switch in Embryonic Expression of the Caenorhabditis Elegans

Ges-1 Gene Centers on Two GATA Sequences." *Developmental Biology* 170(2):397–419. doi: 10.1006/dbio.1995.1225.

Elferink, Jan GR. 1999. "Thimerosal A Versatile Sulfhydryl Reagent, Calcium Mobilizer, and Cell Function-Modulating Agent." *General Pharmacology* 33(1):1–6. doi: 10.1016/S0306-3623(98)00258-4.

Fares, Hanna, and Iva Greenwald. 2001. "Genetic Analysis of Endocytosis in Caenorhabditis Elegans: Coelomocyte Uptake Defective Mutants." *Genetics (Austin)* 159(1):133–45. doi: 10.1093/genetics/159.1.133.

Ferri, Domenico, Amelia Mazzone, Giuseppa Esterina Liquori, Grazia Cassano, Maria Svelto, and Giuseppe Calamita. 2003. "Ontogeny, Distribution, and Possible Functional Implications of an Unusual Aquaporin, AQP8, in Mouse Liver." *Hepatology (Baltimore, Md.)* 38(4):947–57. doi: 10.1053/jhep.2003.50397.

Fridovich, Irwin. 1995. "Superoxide Radical and Superoxide Dismutases." *Annual Review of Biochemistry* 64(1):97–112. doi: 10.1146/annurev.bi.64.070195.000525.

Fridovich, Irwin. 1997. "Superoxide Anion Radical ($O_2^{\cdot-}$), Superoxide Dismutases, and Related Matters." *The Journal of Biological Chemistry* 272(30):18515–17. doi: 10.1074/jbc.272.30.18515.

Fukui, Masayuki, and Bao Ting Zhu. 2010. "Mitochondrial Superoxide Dismutase SOD2, but Not Cytosolic SOD1, Plays a Critical Role in Protection against Glutamate-Induced Oxidative Stress and Cell Death in HT22 Neuronal Cells." *Free Radical Biology and Medicine* 48(6):821–30. doi: 10.1016/j.freeradbiomed.2009.12.024.

Furness, John B., Brid P. Callaghan, Leni R. Rivera, and Hyun-Jung Cho. 2014. "The Enteric Nervous System and Gastrointestinal Innervation: Integrated Local and Central Control." *Advances in Experimental Medicine and Biology* 817:39–71. doi: 10.1007/978-1-4939-0897-4_3.

Gao, Jing, Makiko Hirata, Akiko Mizokami, Jin Zhao, Ichiro Takahashi, Hiroshi Takeuchi, and Masato Hirata. 2016. "Differential Role of SNAP-25 Phosphorylation by Protein Kinases A and C in the Regulation of SNARE Complex Formation and Exocytosis in PC12 Cells." *Cellular Signalling* 28(5):425–37. doi: 10.1016/j.cellsig.2015.12.014.

García Santamarina, Sarela, Susanna Boronat i Llop, and Elena Hidalgo Hernando. 2014. "Reversible Cysteine Oxidation in Hydrogen Peroxide Sensing and Signal Transduction." doi: 10.1021/bi401700f.

Gibbs, James, Robert C. Young, and Gerade P. Smith. 1973. "Cholecystokinin Elicits Satiety in Rats with Open Gastric Fistulas." *Nature (London)* 245(5424):323–25. doi: 10.1038/245323a0.

Giglio, A. M., T. Hunter, J. V. Bannister, W. H. Bannister, and G. J. Hunter. 1994. "The Copper/Zinc Superoxide Dismutase Gene of Caenorhabditis Elegans." *Biochemistry and Molecular Biology International* 33(1):41–44.

Giniatullin, A. R., and R. A. Giniatullin. 2003. "Dual Action of Hydrogen Peroxide on Synaptic Transmission at the Frog Neuromuscular Junction." *The Journal of Physiology* 552(1):283–93. doi: 10.1113/jphysiol.2003.050690.

Giniatullin, Arthur, Alexey Petrov, and Rashid Giniatullin. 2019. "Action of Hydrogen Peroxide on Synaptic Transmission at the Mouse Neuromuscular Junction." *Neuroscience* 399:135–45. doi: 10.1016/j.neuroscience.2018.12.027.

Goda, Yukiko. 1997. "SNAREs and Regulated Vesicle Exocytosis." *Proceedings of the National Academy of Sciences - PNAS* 94(3):769–72. doi: 10.1073/pnas.94.3.769.

Grenham, Sue, Gerard Clarke, John F. Cryan, and Timothy G. Dinan. 2011. "Brain-Gut-Microbe Communication in Health and Disease." *Frontiers in Physiology* 2:94–94. doi: 10.3389/fphys.2011.00094.

Haber, Adam L., Moshe Biton, Noga Rogel, Rebecca H. Herbst, Karthik Shekhar, Christopher Smillie, Grace Burgin, Toni M. Delorey, Michael R. Howitt, Yarden Katz, Itay Tirosh, Semir Beyaz, Danielle Dionne, Mei Zhang, Raktima Raychowdhury, Wendy S. Garrett, Orit Rozenblatt-Rosen, Hai Ning Shi, Omer Yilmaz, Ramnik J. Xavier, and Aviv Regev. 2017. "A Single-Cell Survey of the Small Intestinal Epithelium." *Nature (London)* 551(7680):333–39. doi: 10.1038/nature24489.

Han, Derick, Fernando Antunes, Raffaella Canali, Daniel Rettori, and Enrique Cadenas. 2003. "Voltage-Dependent Anion Channels Control the Release of the Superoxide Anion from Mitochondria to Cytosol." *The Journal of Biological Chemistry* 278(8):5557–63. doi: 10.1074/jbc.M210269200.

Han, Seong-Kyu, Michelle L. Gottsch, Kathy J. Lee, Simina M. Popa, Jeremy T. Smith, Sonya K. Jakawich, Donald K. Clifton, Robert A. Steiner, and Allan E. Herbison. 2005. "Activation of Gonadotropin-Releasing Hormone Neurons by Kisspeptin as a Neuroendocrine Switch for the Onset of Puberty." *The Journal of Neuroscience* 25(49):11349–56. doi: 10.1523/JNEUROSCI.3328-05.2005.

Han, Wenfei, Luis A. Tellez, Matthew H. Perkins, Isaac O. Perez, Taoran Qu, Jozelia Ferreira, Tatiana L. Ferreira, Daniele Quinn, Zhong-Wu Liu, Xiao-Bing Gao, Melanie M. Kaelberer, Diego V. Bohórquez, Sara J. Shammah-Lagnado, Guillaume de Lartigue, and Ivan E. de Araujo. 2018. "A Neural Circuit for Gut-Induced Reward." *Cell* 175(3):665-678.e23. doi: 10.1016/j.cell.2018.08.049.

Hourihan, John M., Lorenza E. Moronetti Mazzeo, L. Paulette Fernández-Cárdenas, and T. Keith Blackwell. 2016. "Cysteine Sulfenylation Directs IRE-1 to Activate the SKN-1/Nrf2 Antioxidant Response." *Molecular Cell* 63(4):553–66. doi: 10.1016/j.molcel.2016.07.019.

Islas-Trejo, A., M. Land, I. Tcherepanova, J. H. Freedman, and C. S. Rubin. 1997. "Structure and Expression of the Caenorhabditis Elegans Protein Kinase C2 Gene. Origins and Regulated Expression of a Family of Ca2+-Activated Protein Kinase C Isoforms." *The Journal of Biological Chemistry* 272(10):6629–40. doi: 10.1074/jbc.272.10.6629.

Iwasaki, Kouichi, Jane Staunton, Owais Saifee, Michael Nonet, and James H. Thomas. 1997. "Aex-3 Encodes a Novel Regulator of Presynaptic Activity in C. Elegans." *Neuron (Cambridge, Mass.)* 18(4):613–22. doi: 10.1016/S0896-6273(00)80302-5.

Jahn, Reinhard, and Richard H. Scheller. 2006. "SNAREs - Engines for Membrane Fusion." *Nature Reviews. Molecular Cell Biology* 7(9):631–43. doi: 10.1038/nrm2002.

Jia, Qi, and Derek Sieburth. 2021. "Mitochondrial Hydrogen Peroxide Positively Regulates Neuropeptide Secretion during Diet-Induced Activation of the Oxidative Stress Response." *Nature Communications* 12(1):2304–2304. doi: 10.1038/s41467-021-22561-x.

Jiménez-Hidalgo, María, Cyril Léopold Kurz, José Rafael Pedrajas, Francisco José Naranjo-Galindo, María González-Barrios, Juan Cabello, Alberto G. Sáez, Encarnación Lozano, Emma L. Button, Elizabeth A. Veal, Juan Carlos Fierro-González, Peter Swoboda, and Antonio Miranda-Vizuete. 2014. "Functional Characterization of Thioredoxin 3 (TRX-3), a Caenorhabditis Elegans Intestine-Specific Thioredoxin." *Free Radical Biology & Medicine* 68(100):205–19. doi: 10.1016/j.freeradbiomed.2013.11.023.

Johnson, Joanne E., Jennifer Giorgione, and Alexandra C. Newton. 2000. "The C1 and C2 Domains of Protein Kinase C Are Independent Membrane Targeting Modules, with Specificity for Phosphatidylserine Conferred by the C1 Domain." *Biochemistry (Easton)* 39(37):11360–69. doi: 10.1021/bi000902c.

Kageyama, Natsumi, Masayo Nose, Masahiro Ono, Yohei Matsunaga, Takashi Iwasaki, and Tsuyoshi Kawano. 2022. "The FMRFamide-like Peptide FLP-2 Is Involved in the Modulation of Larval Development and Adult Lifespan by Regulating the Secretion of the Insulin-like Peptide INS-35 in Caenorhabditis Elegans." *Bioscience, Biotechnology, and Biochemistry* 86(9):1231–39. doi: 10.1093/bbb/zbac108.

Kamata, Hideaki, Tomoyuki Manabe, Shin-ichi Oka, Keiko Kamata, and Hajime Hirata. 2002. "Hydrogen Peroxide Activates IκB Kinases through Phosphorylation of Serine Residues in the Activation Loops." *FEBS Letters* 519(1):231–37. doi: 10.1016/S0014-5793(02)02712-6.

Kamath, R. 2003. "Genome-Wide RNAi Screening in Caenorhabditis Elegans." *Methods (San Diego, Calif.)* 30(4):313–21. doi: 10.1016/s1046-2023(03)00050-1.

Kemble, David J., and Gongqin Sun. 2009. "Direct and Specific Inactivation of Protein Tyrosine Kinases in the Src and FGFR Families by Reversible Cysteine Oxidation." *Proceedings of the National Academy of Sciences - PNAS* 106(13):5070–75. doi: 10.1073/pnas.0806117106.

Kim, Ki Mo, Deok Rim Heo, Young-A. Kim, Jun Lee, No Soo Kim, and Ok-Sun Bang. 2016. "Coniferaldehyde Inhibits LPS-Induced Apoptosis through the PKC α/β II/Nrf-2/HO-1 Dependent Pathway in RAW264.7 Macrophage Cells." *Environmental Toxicology and Pharmacology* 48:85–93. doi: 10.1016/j.etap.2016.10.016.

Knoefler, Daniela, Maike Thamsen, Martin Koniczek, Nicholas J. Niemuth, Ann-Kristin Diederich, and Ursula Jakob. 2012. "Quantitative In Vivo Redox Sensors Uncover Oxidative Stress as an Early Event in Life." *Molecular Cell* 47(5):767–76. doi: 10.1016/j.molcel.2012.06.016.

Konishi, Hiroaki, Motonari Tanaka, Yukitoshi Takemura, Hidenori Matsuzaki, Yoshitaka Ono, Ushio Kikkawa, and Yasutomi Nishizuka. 1997. "Activation of Protein Kinase C by Tyrosine Phosphorylation in Response to H2O2." *Proceedings of the National Academy of Sciences - PNAS* 94(21):11233–37. doi: 10.1073/pnas.94.21.11233.

Konishi, Hiroaki, Emiko Yamauchi, Hisaaki Taniguchi, Toshiyoshi Yamamoto, Hidenori Matsuzaki, Yukitoshi Takemura, Kyoko Ohmae, Ushio Kikkawa, and Yasutomi Nishizuka. 2001. "Phosphorylation Sites of Protein Kinase C δ in H2O2-Treated Cells and Its Activation by Tyrosine Kinase in Vitro." *Proceedings of the National Academy of Sciences - PNAS* 98(12):6587–92. doi: 10.1073/pnas.111158798.

Kontos, Hermes A., Enoch P. Wei, Earl F. Ellis, Larry W. Jenkins, John T. Povlishock, G. Thomas Rowe, and Michael L. Hess. 1985. “Appearance of Superoxide Anion Radical in Cerebral Extracellular Space during Increased Prostaglandin Synthesis in Cats.” *Circulation Research* 57(1):142–51. doi: 10.1161/01.RES.57.1.142.

Lai, N. Y., K. Mills, and I. M. Chiu. 2017. “Sensory Neuron Regulation of Gastrointestinal Inflammation and Bacterial Host Defence.” *Journal of Internal Medicine* 282(1):5–23. doi: 10.1111/joim.12591.

Land, Marianne, and Charles S. Rubin. 2017. “A Calcium- and Diacylglycerol-Stimulated Protein Kinase C (PKC), Caenorhabditis Elegans PKC-2, Links Thermal Signals to Learned Behavior by Acting in Sensory Neurons and Intestinal Cells.” *Molecular and Cellular Biology* 37(19). doi: 10.1128/MCB.00192-17.

Larsen, Martha J., Elizabeth Ruiz Lancheros, Tracey Williams, David E. Lowery, Timothy G. Geary, and Teresa M. Kubiak. 2013. “Functional Expression and Characterization of the C. Elegans G-Protein-Coupled FLP-2 Receptor (T19F4.1) in Mammalian Cells and Yeast.” *International Journal for Parasitology -- Drugs and Drug Resistance* 3:1–7. doi: 10.1016/j.ijpddr.2012.10.002.

Lee, Kiho, and Eleftherios Mylonakis. 2017. “An Intestine-Derived Neuropeptide Controls Avoidance Behavior in Caenorhabditis Elegans.” *Cell Reports (Cambridge)* 20(10):2501–12. doi: 10.1016/j.celrep.2017.08.053.

Lee, Yoon-Jin, Hae-Nyun Cho, Jae-Won Soh, Gil Ja Jhon, Chul-Koo Cho, Hee-Yong Chung, Sangwoo Bae, Su-Jae Lee, and Yun-Sil Lee. 2003. “Oxidative Stress-Induced Apoptosis Is Mediated by ERK1/2 Phosphorylation.” *Experimental Cell Research* 291(1):251–66. doi: 10.1016/S0014-4827(03)00391-4.

Li, Guang, Jianke Gong, Haoyun Lei, Jianfeng Liu, and X. Z. Shawn Xu. 2016. “Promotion of Behavior and Neuronal Function by Reactive Oxygen Species in C. Elegans.” *Nature Communications* 7(1):13234. doi: 10.1038/ncomms13234.

Li, Zongwei, Yong Gu, Ruoxue Wen, Fanxia Shen, Heng-Li Tian, Guo-Yuan Yang, and Zhijun Zhang. 2019. “Lysosome Exocytosis Is Involved in Astrocyte ATP Release after Oxidative Stress Induced by H2O2.” *Neuroscience Letters* 705:251–58. doi: 10.1016/j.neulet.2019.03.046.

Lin-Moore, Alexander T., Motunrayo J. Oyeyemi, and Marc Hammarlund. 2021. “Rab-27 Acts in an Intestinal Pathway to Inhibit Axon Regeneration in C. Elegans.” *PLoS Genetics* 17(11):e1009877–e1009877. doi: 10.1371/journal.pgen.1009877.

Liu, D. W., and J. H. Thomas. 1994. “Regulation of a Periodic Motor Program in C. Elegans.” *The Journal of Neuroscience* 14(4):1953–62. doi: 10.1523/jneurosci.14-04-01953.1994.

Liu, Junqiang, Pei Zhang, Zhongfan Zheng, Muhammad Irfan Afridi, Shan Zhang, Zhiqing Wan, Xiumei Zhang, Lukas Stingelin, Yirong Wang, and Haijun Tu. 2023. “GABAergic Signaling between Enteric Neurons and Intestinal Smooth Muscle Promotes Innate Immunity and Gut Defense in Caenorhabditis Elegans.” *Immunity* 56(7):1515-1532.e9. doi: 10.1016/j.immuni.2023.06.004.

Lutz, T. A., E. Del Prete, and E. Scharrer. 1994. “Reduction of Food Intake in Rats by Intraperitoneal Injection of Low Doses of Amylin.” *Physiology & Behavior* 55(5):891–95. doi: 10.1016/0031-9384(94)90076-0.

Lutz, T. A., N. Geary, M. M. Szabady, E. Del Prete, and E. Scharrer. 1995. “Amylin Decreases Meal Size in Rats.” *Physiology & Behavior* 58(6):1197–1202. doi: 10.1016/0031-9384(95)02067-5.

Mahoney, Timothy R., Qiang Liu, Takashi Itoh, Shuo Luo, Gayla Hadwiger, Rose Vincent, Zhao-Wen Wang, Mitsunori Fukuda, and Michael L. Nonet. 2006. “Regulation of Synaptic Transmission by RAB-3 and RAB-27 in Caenorhabditis Elegans.” *Molecular Biology of the Cell* 17(6):2617–25. doi: 10.1091/mbc.E05-12-1170.

Mahoney, Timothy R., Shuo Luo, Elaine K. Round, Martin Brauner, Alexander Gottschalk, James H. Thomas, and Michael L. Nonet. 2008. “Intestinal Signaling to GABAergic Neurons Regulates a Rhythmic Behavior in Caenorhabditis Elegans.” *Proceedings of the National Academy of Sciences - PNAS* 105(42):16350–55. doi: 10.1073/pnas.0803617105.

Maman, Moria, Filipa Carvalhal Marques, Yuli Volovik, Tatyana Dubnikov, Michal Bejerano-Sagie, and Ehud Cohen. 2013. “A Neuronal GPCR Is Critical for the Induction of the Heat Shock Response in the Nematode C. Elegans.” *The Journal of Neuroscience* 33(14):6102–11. doi: 10.1523/JNEUROSCI.4023-12.2013.

Marinho, H. Susana, Carla Real, Luísa Cyrne, Helena Soares, and Fernando Antunes. 2014. “Hydrogen Peroxide Sensing, Signaling and Regulation of Transcription Factors.” *Redox Biology* 2(C):535–62. doi: 10.1016/j.redox.2014.02.006.

Mayer, Emeran A., Karina Nance, and Shelley Chen. 2022. “The Gut-Brain Axis.” *Annual Review of Medicine* 73(1):439–53. doi: 10.1146/annurev-med-042320-014032.

Mehrian-Shai, Ruty, Juergen K. V. Reichardt, Curtis C. Harris, and Amos Toren. 2019. “The Gut-Brain Axis, Paving the Way to Brain Cancer.” *Trends in Cancer* 5(4):200–207. doi: 10.1016/j.trecan.2019.02.008.

Mello, C. C., J. M. Kramer, D. Stinchcomb, and V. Ambros. 1991. “Efficient Gene Transfer in C.Elegans: Extrachromosomal Maintenance and Integration of Transforming Sequences.” *The EMBO Journal* 10(12):3959–70. doi: 10.1002/j.1460-2075.1991.tb04966.x.

Mertens, Inge, Tom Meeusen, Tom Janssen, Ronald Nachman, and Liliane Schoofs. 2005. “Molecular Characterization of Two G Protein-Coupled Receptor Splice Variants as FLP2 Receptors in Caenorhabditis Elegans.” *Biochemical and Biophysical Research Communications* 330(3):967–74. doi: 10.1016/j.bbrc.2005.03.071.

Messner, Kevin R., and James A. Imlay. 2002. “Mechanism of Superoxide and Hydrogen Peroxide Formation by Fumarate Reductase, Succinate Dehydrogenase, and Aspartate Oxidase.” *The Journal of Biological Chemistry* 277(45):42563–71. doi: 10.1074/jbc.M204958200.

Miller, Brittany M., Megan J. Liou, Lillian F. Zhang, Henry Nguyen, Yael Litvak, Eva-Magdalena Schorr, Kyung Ku Jang, Connor R. Tiffany, Brian P. Butler, and Andreas J. Bäumler. 2020. “Anaerobic Respiration of NOX1-Derived Hydrogen Peroxide Licenses Bacterial Growth at the Colonic Surface.” *Cell Host & Microbe* 28(6):789-797.e5. doi: 10.1016/j.chom.2020.10.009.

Min, Do Sik, Eung-Gook Kim, and John H. Exton. 1998. “Involvement of Tyrosine Phosphorylation and Protein Kinase C in the Activation of Phospholipase D by H2O2 in Swiss 3T3 Fibroblasts.” *The Journal of Biological Chemistry* 273(45):29986–94. doi: 10.1074/jbc.273.45.29986.

Miranda-Vizuete, Antonio, Anastasios E. Damdimopoulos, and Giannis Spyrou. 2000. “The Mitochondrial Thioredoxin System.” *Antioxidants & Redox Signaling* 2(4):801–10. doi: 10.1089/ars.2000.2.4-801.

Murphy, Coleen T., Seung-Jae Lee, and Cynthia Kenyon. 2007. “Tissue Entrainment by Feedback Regulation of Insulin Gene Expression in the Endoderm of Caenorhabditis Elegans.” *Proceedings of the National Academy of Sciences - PNAS* 104(48):19046–50. doi: 10.1073/pnas.0709613104.

Nagy, Gabor, Ulf Matti, Ralf B. Nehring, Thomas Binz, Jens Rettig, Erwin Neher, and Jakob B. Sorensen. 2002. “Protein Kinase C-Dependent Phosphorylation of Synaptosome-Associated Protein of 25 kDa at Ser187 Potentiates Vesicle Recruitment.” *The Journal of Neuroscience* 22(21):9278–86. doi: 10.1523/JNEUROSCI.22-21-09278.2002.

Nebigil, Canan G. 1997. “Suppression of Phospholipase C β, γ, and δ Families Alters Cell Growth and Phosphatidylinositol 4,5-Bisphosphate Levels.” *Biochemistry (Easton)* 36(50):15949–58. doi: 10.1021/bi971721m.

Nelson, Kimberly J., Jesalyn A. Bolduc, Hanzhi Wu, John A. Collins, Elizabeth A. Burke, Julie A. Reisz, Chananat Klomsiri, Scott T. Wood, Raghunatha R. Yammani, Leslie B. Poole, Cristina M. Furdui, and Richard F. Loeser. 2018. “H2O2 Oxidation of Cysteine Residues in C-Jun N-Terminal Kinase 2 (JNK2) Contributes to Redox Regulation in Human Articular Chondrocytes.” *The Journal of Biological Chemistry* 293(42):16376–89. doi: 10.1074/jbc.RA118.004613.

Netto, Luis E. S., and Fernando Antunes. 2016. “The Roles of Peroxiredoxin and Thioredoxin in Hydrogen Peroxide Sensing and in Signal Transduction.” *Molecules and Cells* 39(1):65–71. doi: 10.14348/molcells.2016.2349.

Nonet, Michael L., Jane E. Staunton, Michael P. Kilgard, Tim Fergestad, Erika Hartwieg, H. Robert Horvitz, Erik M. Jorgensen, and Barbara J. Meyer. 1997. “Caenorhabditis Elegans Rab-3 Mutant Synapses Exhibit Impaired Function and Are Partially Depleted of Vesicles.” *The Journal of Neuroscience* 17(21):8061–73. doi: 10.1523/jneurosci.17-21-08061.1997.

O’Donnell, Michael P., Pin-Hao Chao, Jan E. Kammenga, and Piali Sengupta. 2018. “Rictor/TORC2 Mediates Gut-to-Brain Signaling in the Regulation of Phenotypic Plasticity in C. Elegans.” *PLoS Genetics* 14(2):e1007213–e1007213. doi: 10.1371/journal.pgen.1007213.

Oláhová, Monika, Sarah R. Taylor, Siavash Khazaipoul, Jinling Wang, Brian A. Morgan, Kunihiro Matsumoto, T. Keith Blackwell, and Elizabeth A. Veal. 2008. “Redox-Sensitive Peroxiredoxin That Is Important for Longevity Has Tissue- and Stress-Specific Roles in Stress Resistance.” *Proceedings of the National Academy of Sciences - PNAS* 105(50):19839–44. doi: 10.1073/pnas.0805507105.

Oláhová, Monika, and Elizabeth A. Veal. 2015. “A Peroxiredoxin, PRDX-2, Is Required for Insulin Secretion and Insulin/IIS-dependent Regulation of Stress Resistance and Longevity.” *Aging Cell* 14(4):558–68. doi: 10.1111/acel.12321.

Oliveira-Marques, Virgínia, H. Susana Marinho, Luísa Cyrne, and Fernando Antunes. 2009. “Role of Hydrogen Peroxide in NF-κB Activation: From Inducer to Modulator.” *Antioxidants & Redox Signaling* 11(9):2223–43. doi: 10.1089/ars.2009.2601.

Ono, Yoshitaka, Tomoko Fujii, Koichi Igarashi, Takayoshi Kuno, Chikako Tanaka, Ushio Kikkawa, and Yasutomi Nishizuka. 1989. “Phorbol Ester Binding to Protein Kinase C Requires a Cysteine-Rich Zinc-Finger-Like Sequence.” *Proceedings of the National Academy of Sciences - PNAS* 86(13):4868–71. doi: 10.1073/pnas.86.13.4868.

Ouaakki, Hafsa, Heetanshi Joshi, Laxmi Rathor, and Sung Min Han. 2023. “Frpr-18, a Neuropeptide Receptor, Regulates Organismal Lifespan and Stress Tolerance in C. Elegans.” *microPublication Biology* 2023. doi: 10.17912/micropub.biology.000840.

Pak, Valeriy V., Daria Ezeriņa, Olga G. Lyublinskaya, Brandán Pedre, Pyotr A. Tyurin-Kuzmin, Natalie M. Mishina, Marion Thauvin, David Young, Khadija Wahni, Santiago Agustín Martínez Gache, Alexandra D. Demidovich, Yulia G. Ermakova, Yulia D. Maslova, Arina G. Shokhina, Emrah Eroglu, Dmitry S. Bilan, Ivan Bogeski, Thomas Michel, Sophie Vriz, Joris Messens, and Vsevolod V. Belousov. 2020. “Ultrasensitive Genetically Encoded Indicator for Hydrogen Peroxide Identifies Roles for the Oxidant in Cell Migration and Mitochondrial Function.” *Cell Metabolism* 31(3):642-653.e6. doi: 10.1016/j.cmet.2020.02.003.

Pang, Shanshan, and Sean P. Curran. 2014. “Adaptive Capacity to Bacterial Diet Modulates Aging in C. Elegans.” *Cell Metabolism* 19(2):221–31. doi: 10.1016/j.cmet.2013.12.005.

Papa, Luena, Giovanni Manfredi, and Doris Germain. 2014. “SOD1, an Unexpected Novel Target for Cancer Therapy.” *Genes & Cancer* 5(1–2):15–21. doi: 10.18632/genesandcancer.4.

Prahlad, Veena, Tyler Cornelius, and Richard I. Morimoto. 2008. “Regulation of the Cellular Heat Shock Response in Caenorhabditis Elegans by Thermosensory Neurons.” *Science (American Association for the Advancement of Science)* 320(5877):811–14. doi: 10.1126/science.1156093.

Satoh, Yohsuke, Hirofumi Sato, Hirofumi Kunitomo, Xianfeng Fei, Koichi Hashimoto, and Yuichi Iino. 2014. “Regulation of Experience-Dependent Bidirectional Chemotaxis by a Neural Circuit Switch in Caenorhabditis Elegans.” *The Journal of Neuroscience* 34(47):15631–37. doi: 10.1523/JNEUROSCI.1757-14.2014.

Shakirzyanova, A. V., A. I. Malomouzh, N. V. Naumenko, and E. E. Nikolsky. 2009. “The Effect of Hydrogen Peroxide on Spontaneous Quantal and Nonquantal Acetylcholine Release from Rat Motor Nerve Endings.” *Doklady. Biological Sciences* 424(1):18–20. doi: 10.1134/S0012496609010062.

Shao, Li-Wa, Rong Niu, and Ying Liu. 2016. “Neuropeptide Signals Cell Non-Autonomous Mitochondrial Unfolded Protein Response.” *Cell Research* 26(11):1182–96. doi: 10.1038/cr.2016.118.

Sharpe, Martyn A., Andrew D. Livingston, and David S. Baskin. 2012. “Thimerosal-Derived Ethylmercury Is a Mitochondrial Toxin in Human Astrocytes: Possible Role of Fenton Chemistry in the Oxidation and Breakage of mtDNA.” *Journal of Toxicology* 2012:373678–373678. doi: 10.1155/2012/373678.

Shi, Yanjun, Lu Qin, Mengting Wu, Junyu Zheng, Tao Xie, and Zhiyong Shao. 2022. “Gut Neuroendocrine Signaling Regulates Synaptic Assembly in C. Elegans.” *EMBO Reports* 23(8):e53267-n/a. doi: 10.15252/embr.202153267.

Shu, Yilong, Xin Liu, Yan Yang, Masami Takahashi, and Kevin D. Gillis. 2008. “Phosphorylation of SNAP-25 at Ser187 Mediates Enhancement of Exocytosis by a Phorbol Ester in INS-1 Cells.” *The Journal of Neuroscience* 28(1):21–30. doi: 10.1523/JNEUROSCI.2352-07.2008.

Sieburth, Derek, Jon M. Madison, and Joshua M. Kaplan. 2006. “PKC-1 Regulates Secretion of Neuropeptides.” *Nature Neuroscience* 10(1):49–57. doi: 10.1038/nn1810.

Singh, Jogender, and Alejandro Aballay. 2019. “Intestinal Infection Regulates Behavior and Learning via Neuroendocrine Signaling.” *eLife* 8. doi: 10.7554/eLife.50033.

Song, Youngmi, Jacqueline A. Koehler, Laurie L. Baggio, Alvin C. Powers, Darleen A. Sandoval, and Daniel J. Drucker. 2019. “Gut-Proglucagon-Derived Peptides Are Essential for Regulating Glucose Homeostasis in Mice.” *Cell Metabolism* 30(5):976-986.e3. doi: 10.1016/j.cmet.2019.08.009.

Takada, Yasunari, Asok Mukhopadhyay, Gopal C. Kundu, Ganapati H. Mahabeleshwar, Sujay Singh, and Bharat B. Aggarwal. 2003. “Hydrogen Peroxide Activates NF-Kappa B through Tyrosine Phosphorylation of I Kappa B Alpha and Serine Phosphorylation of P65: Evidence for the Involvement of I Kappa B Alpha Kinase and Syk Protein-Tyrosine Kinase.” *The Journal of Biological Chemistry* 278(26):24233–41. doi: 10.1074/jbc.M212389200.

Tao, Jun, Qin-Yi Wu, Yi-Cheng Ma, Yuan-Li Chen, and Cheng-Gang Zou. 2017. “Antioxidant Response Is a Protective Mechanism against Nutrient Deprivation in C. Elegans.” *Scientific Reports* 7(1):43547–43547. doi: 10.1038/srep43547.

Taylor, Seth R., Gabriel Santpere, Alexis Weinreb, Alec Barrett, Molly B. Reilly, Chuan Xu, Erdem Varol, Panos Oikonomou, Lori Glenwinkel, Rebecca McWhirter, Abigail Poff, Manasa Basavaraju, Ibnul Rafi, Eviatar Yemini, Steven J. Cook, Alexander Abrams, Berta Vidal, Cyril Cros, Saeed Tavazoie, Nenad Sestan, Marc Hammarlund, Oliver Hobert, and David M. Miller. 2021. “Molecular Topography of an Entire Nervous System.” *Cell* 184(16):4329-4347.e23. doi: 10.1016/j.cell.2021.06.023.

Thacker, Colin, and Ann M. Rose. 2000. “A Look at the Caenorhabditis Elegans Kex2/Subtilisin-like Proprotein Convertase Family.” *BioEssays* 22(6):545–53. doi: 10.1002/(SICI)1521-1878(200006)22:6<545::AID-BIES7>3.0.CO;2-F.

Thomas, J. H. 1990. “Genetic Analysis of Defecation in Caenorhabditis Elegans.” *Genetics (Austin)* 124(4):855–72. doi: 10.1093/genetics/124.4.855.

Titos, Iris, Alen Juginović, Alexandra Vaccaro, Keishi Nambara, Pavel Gorelik, Ofer Mazor, and Dragana Rogulja. 2023. “A Gut-Secreted Peptide Suppresses Arousability from Sleep.” *Cell* 186(10):2273–74. doi: 10.1016/j.cell.2023.04.005.

Topham, Matthew K. 2006. “Signaling Roles of Diacylglycerol Kinases.” *Journal of Cellular Biochemistry* 97(3):474–84. doi: 10.1002/jcb.20704.

Van, An-Angela N., Maya T. Kunkel, Timothy R. Baffi, Gema Lordén, Corina E. Antal, Sourav Banerjee, and Alexandra C. Newton. 2021. “Protein Kinase C Fusion Proteins Are Paradoxically Loss of Function in Cancer.” *The Journal of Biological Chemistry* 296:100445–100445. doi: 10.1016/j.jbc.2021.100445.

Van Raamsdonk, Jeremy Michael, and Siegfried Hekimi. 2010. “Reactive Oxygen Species and Aging in Caenorhabditis Elegans: Causal or Casual Relationship?” *Antioxidants & Redox Signaling* 13(12):1911–53. doi: 10.1089/ars.2010.3215.

Vincent, Andrea M., James W. Russell, Kelli A. Sullivan, Carey Backus, John M. Hayes, Lisa L. McLean, and Eva L. Feldman. 2007. “SOD2 Protects Neurons from Injury in Cell Culture and Animal Models of Diabetic Neuropathy.” *Experimental Neurology* 208(2):216–27. doi: 10.1016/j.expneurol.2007.07.017.

Vitali, Roberta, Clara Prioreschi, Laura Lorenzo Rebenaque, Eleonora Colantoni, Daniela Giovannini, Sarah Frusciante, Gianfranco Diretto, Francisco Marco-Jiménez, Mariateresa Mancuso, Arianna Casciati, and Simonetta Pazzaglia. 2022. “Gut–Brain Axis: Insights from Hippocampal Neurogenesis and Brain Tumor Development in a Mouse Model of Experimental Colitis Induced by Dextran Sodium Sulfate.” *International Journal of Molecular Sciences* 23(19):11495-. doi: 10.3390/ijms231911495.

Wang, Han, Kelly Girskis, Tom Janssen, Jason P. Chan, Krishnakali Dasgupta, James A. Knowles, Liliane Schoofs, and Derek Sieburth. 2013. “Neuropeptide Secreted from a Pacemaker Activates Neurons to Control a Rhythmic Behavior.” *Current Biology* 23(9):746–54. doi: 10.1016/j.cub.2013.03.049.

Wang, Xiaowen, Hong Zhang, Russell Sapio, Jun Yang, Justin Wong, Xin Zhang, Jessie Y. Guo, Sharon Pine, Holly Van Remmen, Hong Li, Eileen White, Chen Liu, Megerditch Kiledjian, Dimitri G. Pestov, and X. F. Steven Zheng. 2021. “SOD1 Regulates Ribosome Biogenesis in KRAS Mutant Non-Small Cell Lung Cancer.” *Nature Communications* 12(1):2259–2259. doi: 10.1038/s41467-021-22480-x.

West, D. B., D. Fey, and S. C. Woods. 1984. “Cholecystokinin Persistently Suppresses Meal Size but Not Food Intake in Free-Feeding Rats.” *American Journal of Physiology. Regulatory, Integrative and Comparative Physiology* 246(5):776-R787. doi: 10.1152/ajpregu.1984.246.5.r776.

Yanase, Yuhki, Izumi Hide, Shoji Mihara, Yasuhito Shirai, Naoaki Saito, Yoshihiro Nakata, Michihiro Hide, and Norio Sakai. 2011. “A Critical Role of Conventional Protein Kinase C in Morphological Changes of Rodent Mast Cells.” *Immunology and Cell Biology* 89(1):149–59. doi: 10.1038/icb.2010.67.

Yang, Yan, Tim J. Craig, Xiaohui Chen, Leonora F. Ciufo, Masami Takahashi, Alan Morgan, and Kevin D. Gillis. 2007. “Phosphomimetic Mutation of Ser-187 of SNAP-25 Increases Both Syntaxin Binding and Highly Ca2+-Sensitive Exocytosis.” *The Journal of General Physiology* 129(3):233–44. doi: 10.1085/jgp.200609685.

Yu, Hong Bing, Hyungjun Yang, Joannie M. Allaire, Caixia Ma, Franziska A. Graef, Arthur Mortha, Qiaochu Liang, Else S. Bosman, Gregor S. Reid, James A. Waschek, Lisa C. Osborne, Harry Sokol, Bruce A. Vallance, and Kevan Jacobson. 2021. “Vasoactive Intestinal Peptide Promotes Host Defense against Enteric Pathogens by Modulating the Recruitment of Group 3 Innate Lymphoid Cells.” *Proceedings of the National Academy of Sciences - PNAS* 118(41):1-. doi: 10.1073/pnas.2106634118.

Zelko, Igor N., Thomas J. Mariani, and Rodney J. Folz. 2002. “Superoxide Dismutase Multigene Family: A Comparison of the CuZn-SOD (SOD1), Mn-SOD (SOD2), and EC-SOD (SOD3) Gene Structures,

1180 Evolution, and Expression." *Free Radical Biology & Medicine* 33(3):337–49. doi: 10.1016/S0891-
1181 5849(02)00905-X.
1182 Zhang, Fujian, Anna-Lena Ström, Kei Fukada, Sangmook Lee, Lawrence J. Hayward, and Haining Zhu.
1183 2007. "Interaction between Familial Amyotrophic Lateral Sclerosis (ALS)-Linked SOD1 Mutants and the
1184 Dynein Complex." *The Journal of Biological Chemistry* 282(22):16691–99. doi: 10.1074/jbc.M609743200.
1185

Figures

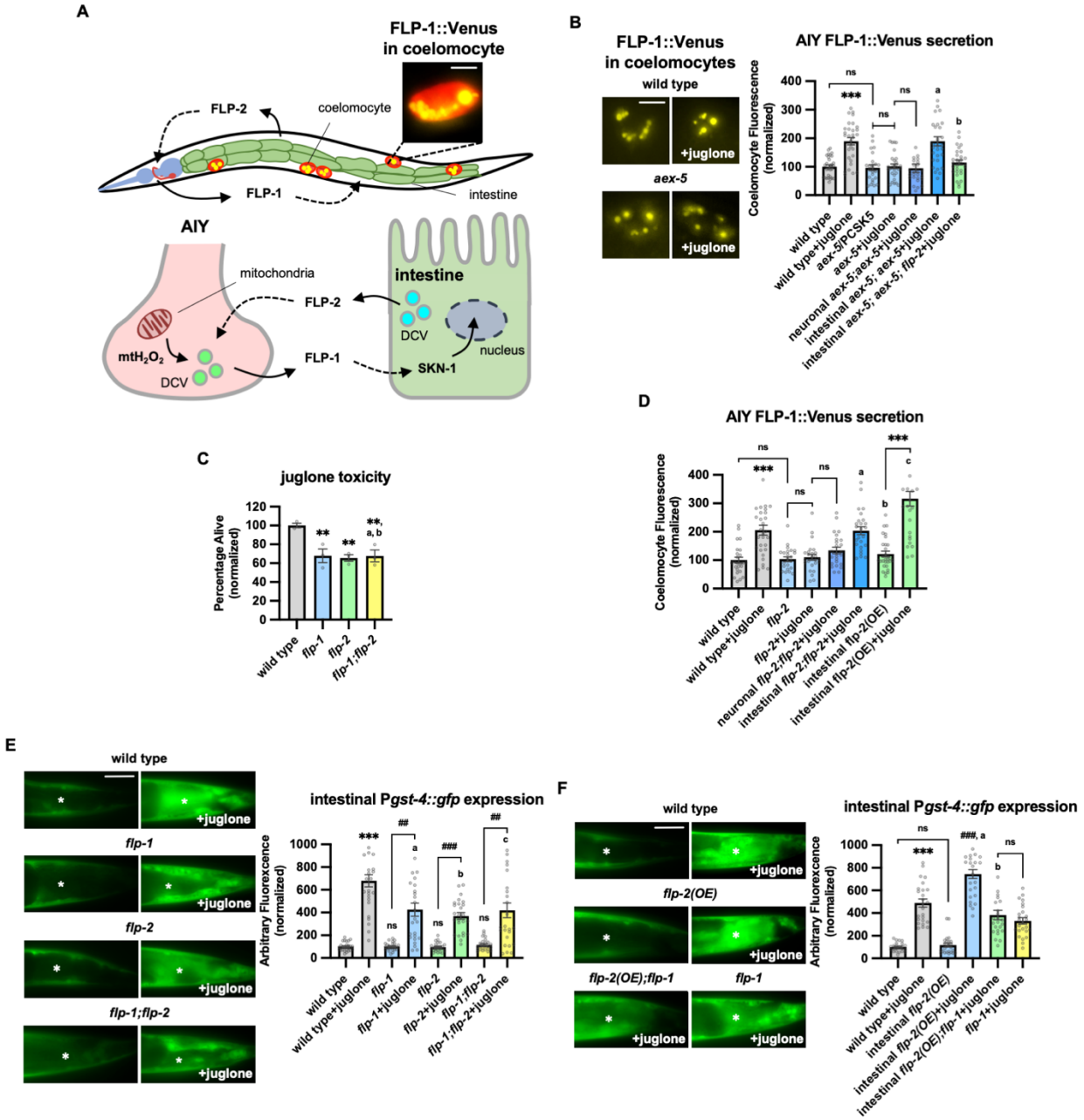

Figure 1. Peptidergic gut-to-neuron FLP-2 signaling potentiates the oxidative stress response.
A (Top) Schematic showing the positions of AIY, intestine and coelomocytes of transgenic animals co-expressing FLP-1::Venus in the intestine and mCherry in coelomocytes. Representative image of the posterior coelomocyte that has taken up Venus into the endocytic compartment. Scale bar: 5μM. (Bottom) Schematic showing FLP-1 and FLP-2 peptides as inter-tissue signals in gut-intestine regulation of the antioxidant response.
B Representative images and quantification of average coelomocyte fluorescence of the indicated mutants expressing FLP-1::Venus fusion proteins in AIY following vehicle M9 or juglone treatment for 10min. Neuronal *aex-5* denotes expression of *aex-5* cDNA under the *rab-3* promoter; intestinal *aex-5* denotes expression of *aex-5* cDNA under the *ges-1* promoter. Unlined *** denotes statistical analysis compared to "wild type"; a denotes statistical analysis compared to "*aex-5*+juglone", $P < 0.001$; b denotes statistical

analysis compared to “intestinal *aex-5; aex-5*+juglone”, $P < 0.01$. n = 30, 30, 24, 30, 26, 30, 30 independent animals. Scale bar: 5μM.

C Average percentage of surviving young adult animals of the indicated genotypes after 16h recovery following 4h juglone treatment. Unlined ** denotes statistical analysis compared to “wild type”, a denotes statistical analysis compared to “*flp-1”*, $P > 0.99$; b denotes statistical analysis compared to “*flp-2”*, $P > 0.99$. n = 213, 156, 189, 195 independent biological samples over three independent experiments.

D Quantification of average coelomocyte fluorescence of the indicated mutants expressing FLP-1::Venus fusion proteins in AIY following M9 or juglone treatment for 10min. Neuronal *flp-2* denotes expression of *flp-2* gDNA under the *rab-3* promoter; intestinal *flp-2* denotes expression of *flp-2* gDNA under the *ges-1* promoter; intestinal *flp-2(OE)* denotes expression of *flp-2* gDNA under the *ges-1* promoter in wild type animals. Unlined *** denotes statistical analysis compared to “wild type”; a denotes statistical analysis compared to “*flp-2*+juglone”, $P < 0.0001$; b denotes statistical analysis compared to “wild type”, $P > 0.99$; c denotes statistical analysis compared to “wild type+juglone”, $P < 0.01$. n = 20, 20, 25, 20, 20, 20, 25, 22 independent animals.

E Representative images and quantification of average fluorescence in the posterior region of transgenic animals expressing P*gst-4::gfp* after 4h vehicle M9 or juglone exposure. Asterisks mark the intestinal region used for quantification. P*gst-4::gfp* expression in the body wall muscles, which appears as fluorescence on the edge animals in some images, was not quantified. Unlined *** and ns denote statistical analysis compared to “wild type”; a, b, and c denote statistical analysis compared to “wild type+juglone”, $P < 0.01$, $P < 0.001$, $P < 0.01$ respectively; unlined ns denotes statistical analysis compared to “wild type”. n = 25, 26, 25, 25, 25, 25, 25, 25 independent animals. Scale bar: 10μM.

F Representative images and quantification of average fluorescence in the posterior region of transgenic animals expressing P*gst-4::gfp* after 4h M9 or juglone exposure. Asterisks mark the intestinal region for quantification. P*gst-4::gfp* expression in the body wall muscles, which appears as fluorescence on the edge animals in some images, was not quantified. Unlined *** denotes statistical analysis compared to “wild type”; unlined ### denotes statistical analysis compared to “wild type+juglone”; a denotes statistical analysis compared to “intestinal *flp-2(OE)*”, $P < 0.0001$; b denotes statistical analysis compared to “intestinal *flp-2(OE)*+juglone”, $P < 0.0001$. n = 23, 25, 25, 26, 24, 25 independent animals. Scale bar: 10μM. Data are mean values ± s.e.m normalized to wild type controls. ns. not significant, ** and ## $P < 0.01$, *** and ### $P < 0.001$ by Brown-Forsythe and Welch ANOVA with Dunnett’s T3 multiple comparisons test.

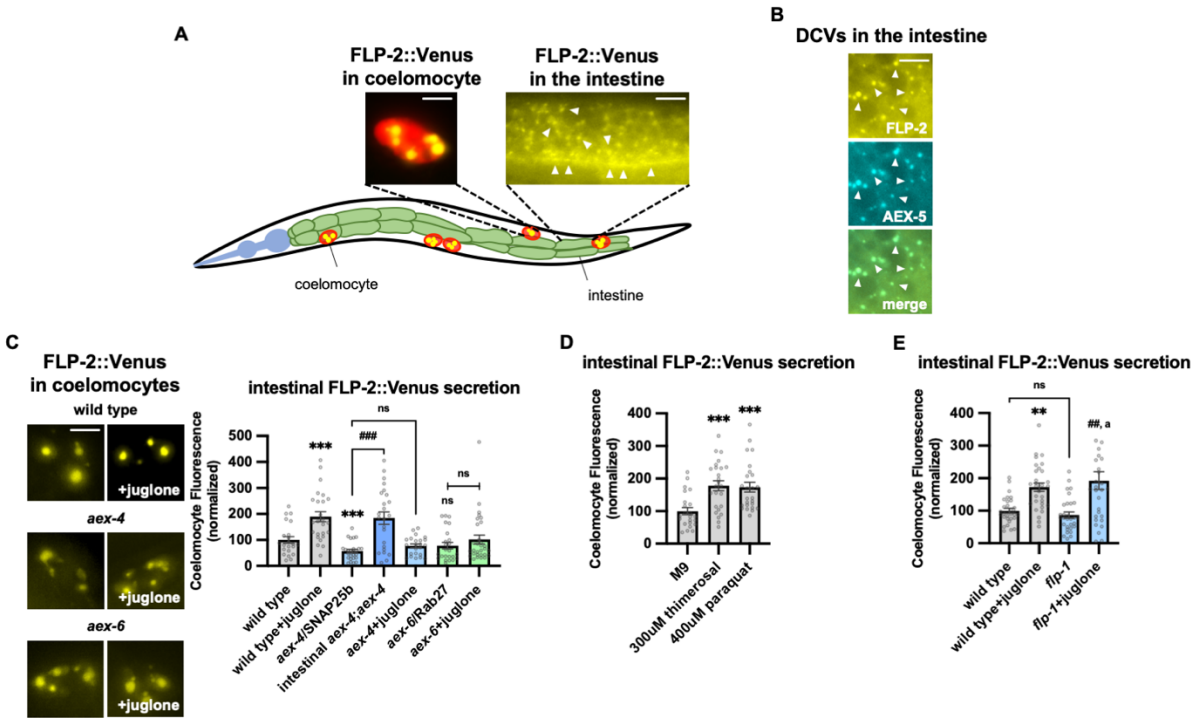

Figure 2. FLP-2 secretion from the intestine is stress regulated.

A Schematic showing the positions of intestine and coelomocytes of transgenic animals co-expressing FLP-2::Venus in the intestine and mCherry in coelomocytes. Representative images of the posterior coelomocyte that have taken up Venus into the endocytic compartment (Scale bar: 5μM) and the posterior intestinal region showing the distribution of FLP-2::Venus in puncta in the intestine are shown (Scale bar: 15μM).

B Representative images of fluorescence distribution in the posterior intestinal region of transgenic animals co-expressing FLP-2::Venus and AEX-5::mTur2 fusion proteins. Arrowheads denote puncta marked by both fusion proteins. Scale bar: 5μM.

C Representative images and quantification of average coelomocyte fluorescence of the indicated mutants expressing FLP-2::Venus fusion proteins in the intestine following M9, juglone or H_2O_2 treatment for 10min. Unlined *** and ns denote statistical analysis compared to "wild type". n = 29, 25, 24, 30, 23, 30, 25, 25, 25 independent animals. Scale bar: 5μM.

D Quantification of average coelomocyte fluorescence of transgenic animals expressing FLP-2::Venus fusion proteins in the intestine following treatment of vehicle (DMSO) or the indicated stressors for 10min. Unlined *** denotes statistical analysis compared to "M9". n = 23, 25, 25 independent animals.

E Quantification of average coelomocyte fluorescence of the indicated mutants expressing FLP-2::Venus fusion proteins in the intestine following M9 or juglone treatment for 10min. Unlined ** denotes statistical analysis compared to "wild type"; unlined ## denotes statistical analysis compared to "*flp-1*"; a denotes statistical analysis compared to "wild type+juglone", $P > 0.90$. n = 30, 30, 30, 30 independent animals. Data are mean values ± s.e.m normalized to wild type controls. ns. not significant, ** and ## $P < 0.01$, *** and ### $P < 0.001$ by Brown-Forsythe and Welch ANOVA with Dunnett's T3 multiple comparisons test.

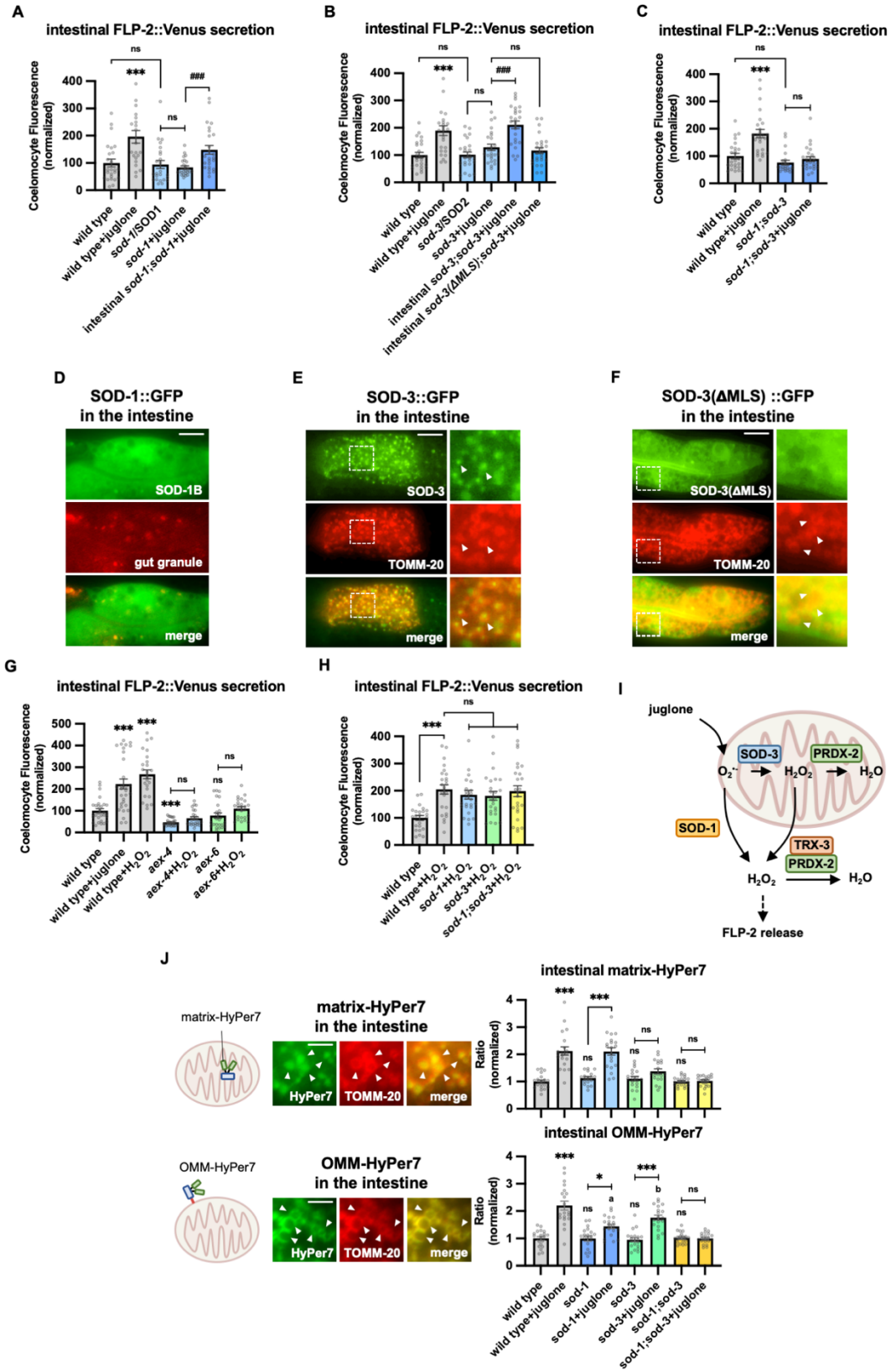

Figure 3. SOD-1/SOD-3 mediates endogenous H_2O_2 regulates FLP-2 release from the intestine.

A Quantification of average coelomocyte fluorescence of the indicated mutants expressing FLP-2::Venus fusion proteins in the intestine following M9 or juglone treatment for 10min. Intestinal *sod*-1 denotes expression of *sod-1b* cDNA under the *ges-1* promoter. Unlined *** denotes statistical analysis compared to "wild type". n = 25, 22, 24, 24, 25 independent animals.
B Quantification of average coelomocyte fluorescence of the indicated mutants expressing FLP-2::Venus fusion proteins in the intestine following M9 or juglone treatment for 10min. Intestinal *sod-3* and *sod-3(*ΔMLS) denote intestinal expression of *sod-3* cDNA and *sod-3(*ΔMLS) variants, which lacks the mitochondrial localization sequence, under the *ges-1* promoter. Unlined *** denotes statistical analysis compared to "wild type". n = 25, 25, 25, 25, 25, 25 independent animals.
C Quantification of average coelomocyte fluorescence of the indicated mutants expressing FLP-2::Venus fusion proteins in the intestine following M9 or juglone treatment for 10min. Unlined *** denotes statistical analysis compared to "wild type". n = 25, 25, 22, 25 independent animals.
D Representative images of fluorescence distribution in the posterior intestinal region of transgenic animals expressing SOD-1b::GFP fusion proteins in contrast against auto-fluorescence of gut granules. Scale bar: 10μM.
E Representative images of fluorescence distribution in the posterior intestinal region of transgenic animals co-expressing SOD-3::GFP and TOMM-20::mCherry (to target mitochondria) fusion proteins. Scale bar: 15μM.
F Representative images of fluorescence distribution in the posterior intestinal region of transgenic animals co-expressing SOD-3(ΔMLS)::GFP and TOMM-20::mCherry fusion proteins. Scale bar: 15μM.
G Quantification of average coelomocyte fluorescence of the indicated mutants expressing FLP-2::Venus fusion proteins in the intestine following M9, juglone or H_2O_2 treatment for 10min. Unlined *** and ns denote statistical analysis compared to "wild type". n = 29, 30, 25, 25, 25, 24, 25 independent animals.
H Quantification of average coelomocyte fluorescence of the indicated mutants expressing FLP-2::Venus fusion proteins in the intestine following M9 or H_2O_2 treatment for 10min. n = independent animals.
I Schematic showing that SOD-1 and SOD-3 mediate juglone-induced H_2O_2 production in promoting FLP-2 release, and the PRDX-2/TRX-3 system detoxifies excessive H_2O_2.
J Schematic, representative images and quantification of fluorescence in the posterior region of the indicated transgenic animals co-expressing mitochondrial matrix targeted HyPer7 (matrix-HyPer7) or mitochondrial outer membrane targeted HyPer7 (OMM-HyPer7) with TOMM-20::mCherry following M9 juglone or H_2O_2 treatment. Unlined *** and ns denote statistical analysis compared to "wild type; a and b denote statistical analysis compared to "wild type+juglone", $P < 0.01$, $P > 0.19$. (top) n = 20, 20, 18, 20, 19, 19, 20, 20 independent animals. (bottom) n = 20, 20, 19, 20, 20, 20, 20, 20 independent animals. Scale bar: 5μM. Data are mean values ± s.e.m normalized to wild type controls. ns. not significant, * $P < 0.05$, *** $P < 0.001$ by Brown-Forsythe and Welch ANOVA with Dunnett's T3 multiple comparisons test.

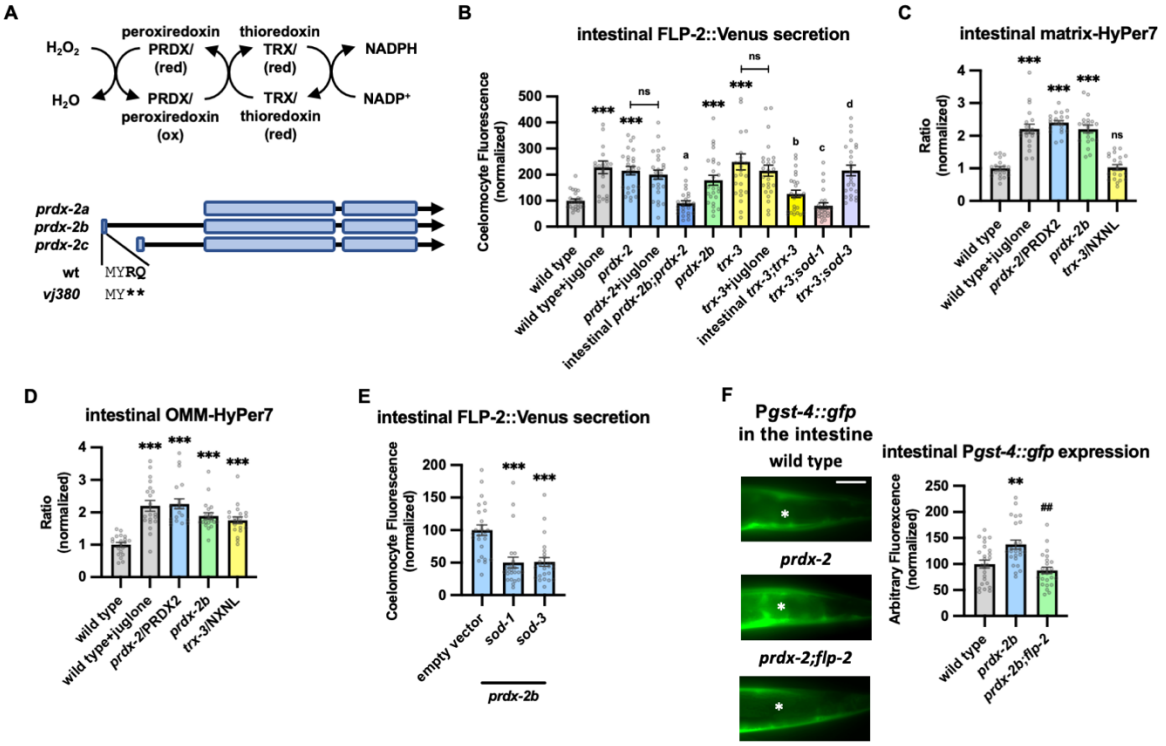

Figure 4. PRDX-2/PRDX and TRX-3/TRX regulate endogenous H_2O_2 and FLP-2 secretion.

A (Top) Schematic showing the PRDX/TRX system in H_2O_2 detoxification. (Bottom) Schematic showing the three isoforms of *prdx-2* transcripts and *vj380* allele of *prdx-2b* knockout.

B Quantification of average coelomocyte fluorescence of the indicated mutants expressing FLP-2::Venus fusion proteins in the intestine following M9 or juglone treatment for 10min. Intestinal *prdx-2b* denotes expression of *prdx-2b* cDNA under the *ges-1* promoter. Intestinal *trx-3* denotes expression of *trx-3* cDNA under the *ges-1* promoter. Unlined *** denotes statistical analysis compared to "wild type"; a denotes statistical analysis compared to "*prdx-2*", $P < 0.0001$; b, c and d denote statistical analysis compared to "*trx-3*", $P < 0.001$, $P < 0.0001$, $P > 0.99$ respectively. n= 25, 23, 25, 25, 25, 25, 25, 25, 25, 25, 25 independent animals.

C and D Quantification of fluorescence in the posterior region of the indicated transgenic animals co-expressing matrix-HyPer7 (C) or OMM-HyPer7 (D) with TOMM-20::mCherry following M9 or juglone treatment. Unlined *** and ns denote statistical analysis compared to "wild type. (C) n = 20, 20, 20, 20, 20 independent animals. (D) n = 20, 20, 20, 20, 20 independent animals.

E Quantification of average coelomocyte FLP-2::Venus fluorescence of transgenic animals fed with RNAi bacteria targeting the indicated genes following M9 treatment for 10min. Unlined *** denotes statistical analysis compared to "empty vector". n = 25, 23, 24 independent animals.

F Representative images and quantification of average fluorescence in the posterior region of transgenic animals expressing P*gst-4::gfp* after 4h M9 or juglone exposure. Asterisks mark the intestinal region for quantification. P*gst-4::gfp* expression in the body wall muscles, which appears as fluorescence on the edge animals in some images, was not quantified. Unlined ** denotes statistical analysis compared to "wild type", unlined ## denotes statistical analysis compared to "*prdx-2b".* n = 25, 25, 25 independent animals. Scale bar: 10μM. Data are mean values ± s.e.m normalized to wild type controls. n.s. not significant, ** and ## $P < 0.01$, *** $P < 0.001$ by Brown-Forsythe and Welch ANOVA with Dunnett's T3 multiple comparisons test.

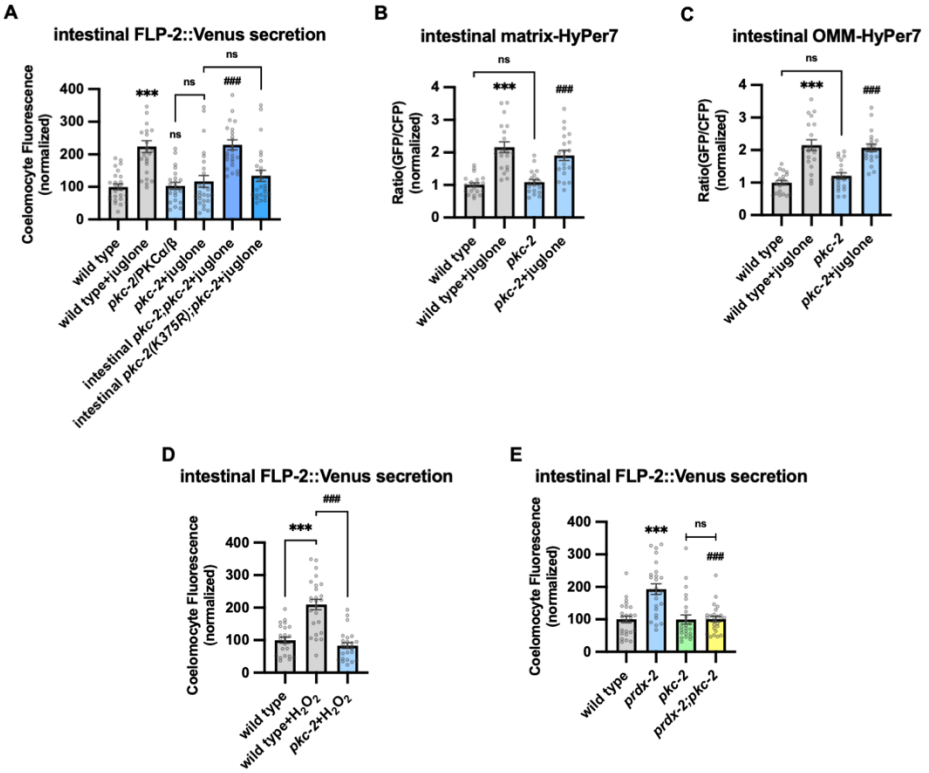

Figure 5. PKC-2/PKCα/β activation by H_2O_2 promotes FLP-2 secretion from the intestine.

A Quantification of average coelomocyte fluorescence of the indicated mutants expressing FLP-2::Venus fusion proteins in the intestine following M9 or juglone treatment for 10min. Intestinal *pkc-2* denotes expression of *pkc-2b cDNA* under the ges-1 promoter. Intestinal *pkc-2b(K375R)* denotes expression of *pkc-2b(K375R)* variants under the *ges-1* promoter. Unlined *** and ns denote statistical analysis compared to "wild type"; ### denote statistical analysis compared to "intestinal *pkc-2b;pkc*-2+juglone". n = 24, 24, 25, 25, 25, 25 independent animals.

B and C Quantification of fluorescence in the posterior region of the indicated transgenic animals co-expressing matrix-HyPer7 (B) or OMM-HyPer7 (C) with TOMM-20::mCherry following M9 or juglone treatment. Unlined *** denotes statistical analysis compared to "wild type"; unlined ### denotes statistical analysis compared to "*pkc-2"*. (B) n = 20, 20, 19, 20 independent animals, (C) n = 20, 20, 20, 20 independent animals.

D Quantification of average coelomocyte fluorescence of the indicated mutants expressing FLP-2::Venus fusion proteins in the intestine following M9 or H_2O_2 treatment for 10min. n = 23, 25, 25 independent animals.

E Quantification of average coelomocyte fluorescence of the indicated mutants expressing FLP-2::Venus fusion proteins in the intestine following M9 treatment for 10min. Unlined *** denotes statistical analysis compared to "wild type"; unlined ### denotes statistical analysis compared to "*prdx-2"*. n = 25, 25, 25, 25 independent animals. Data are mean values ± s.e.m normalized to wild type controls. ns. not significant, *** and ### $P < 0.001$ by Brown-Forsythe and Welch ANOVA with Dunnett's T3 multiple comparisons test.

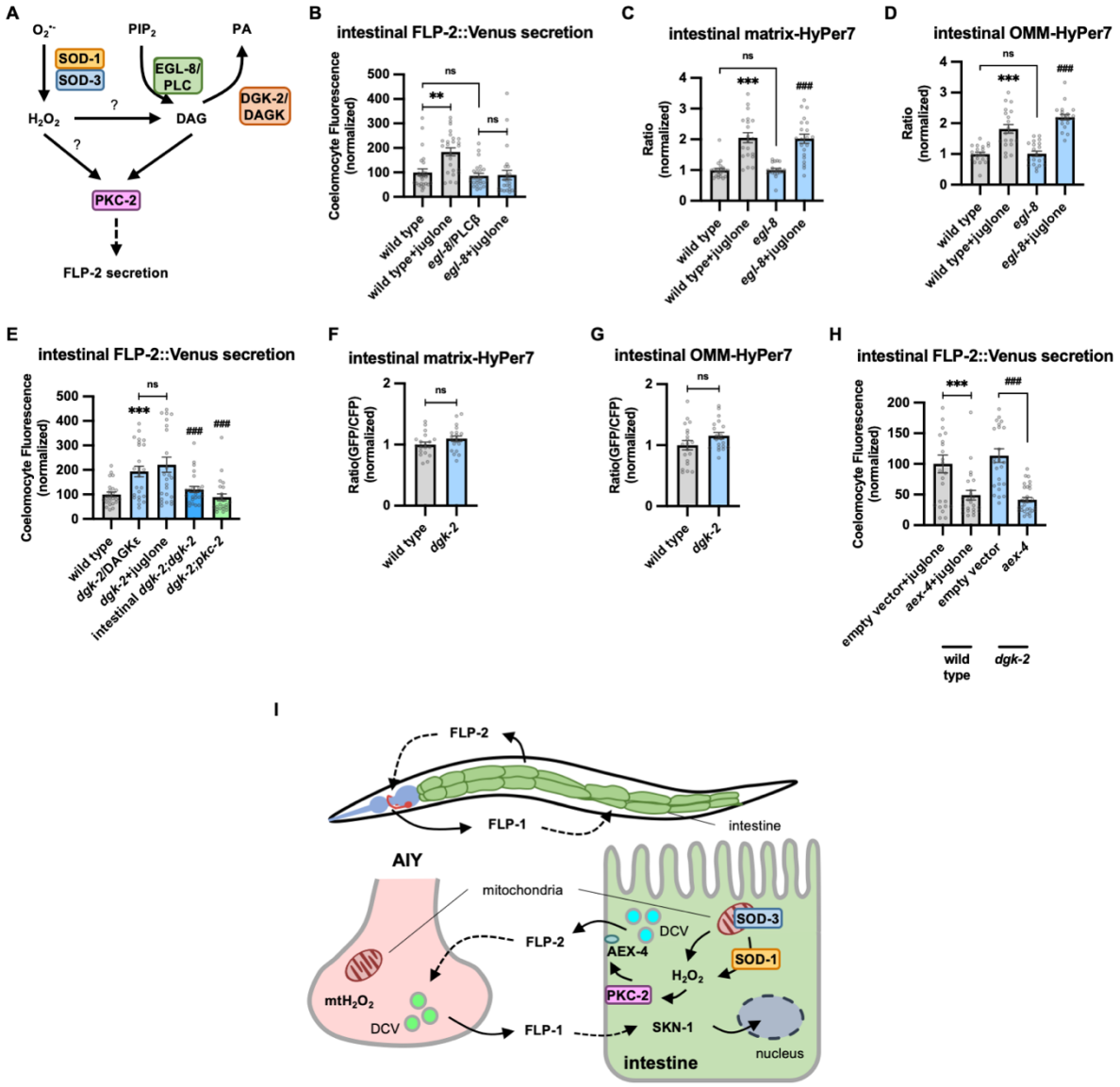

Figure 6. DAG promotes PKC-2 mediated FLP-2 secretion from the intestine.

A Schematic showing PLC and DGK mediates DAG metabolism and DAG functions in H_2O_2-mediated FLP-2 signaling.

B Quantification of average coelomocyte fluorescence of the indicated mutants expressing FLP-2::Venus fusion proteins in the intestine following M9 or juglone treatment for 10min. n = 25, 25, 25, 25 independent animals.

C and D Quantification of fluorescence in the posterior region of the indicated transgenic animals co-expressing matrix-HyPer7 (C) or OMM-HyPer7 (D) with TOMM-20::mCherry following M9 or juglone treatment. Unlined *** denotes statistical analysis compared to "wild type"; unlined ### denotes statistical analysis compared to "*egl-8*". (C) n = 22, 20, 20, 21 independent animals, (D) n = 20, 20, 20, 20 independent animals.

E Quantification of average coelomocyte fluorescence of the indicated mutants expressing FLP-2::Venus fusion proteins in the intestine following M9 or juglone treatment for 10min. Intestinal *dgk-2* denotes expression of *dgk-2a* cDNA under the *ges-1* promoter. Unlined *** denotes statistical analysis compared to "wild type"; unlined ### denotes statistical analysis compared to "*dgk-2*/DGKε". n = 25, 25, 25, 25, 24 independent animals.

1357 **F and G** Quantification of fluorescence in the posterior region of the indicated transgenic animals co-
1358 expressing matrix-HyPer7 (F) or OMM-HyPer7 (G) with TOMM-20::mCherry following M9 treatment. (F) n
1359 = 20, 20 independent animals, (G) n = 20, 20 independent animals.
1360 **H** Quantification of average coelomocyte fluorescence of the indicated transgenic animals fed with RNAi
1361 bacteria targeting the indicated genes in the intestine following M9 treatment for 10min. n = 25, 24, 25, 30
1362 independent animals.
1363 **I** (Top) Schematic showing the position of intestine and AIY neurons in FLP-1-FLP-2 mediated axis. (Bottom)
1364 Schematic showing endogenous H_2O_2 promotes PKC-2/AEX-4 mediated FLP-2 release from the intestine
1365 in FLP-1-FLP-2 regulated inter-tissue axis. Data are mean values ± s.e.m normalized to wild type controls.
1366 ns. not significant, ** $P < 0.01$, *** and ### $P < 0.001$ by Brown-Forsythe and Welch ANOVA with Dunnett's
1367 T3 multiple comparisons test.
1368

1369 **Supplementary Figures**
1370

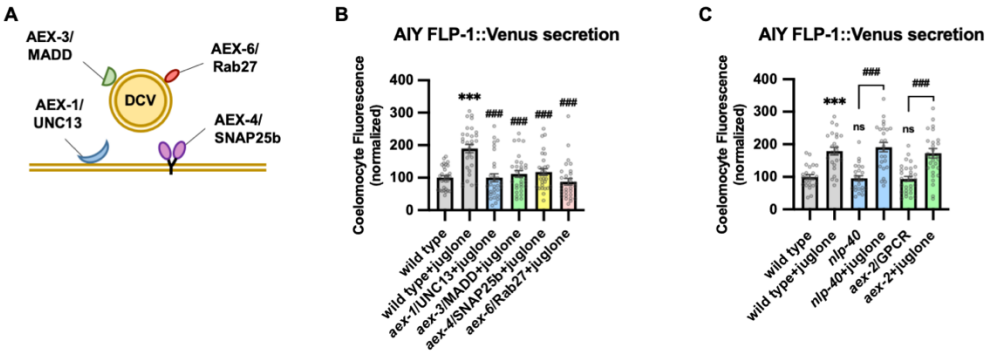

1371
1372 **Supplementary Figure 1. The effect of intestinal DCV secretion mutations on FLP-1 release from AIY.**
1373 **A** Schematic showing the locations of AEX-1/UNC13, AEX-3/MADD, AEX-4/SNAP25 and AEX-6/Rab27
1374 relative to a DCV.
1375 **B** Quantification of average coelomocyte fluorescence of the indicated mutants expressing FLP-1::Venus
1376 fusion proteins in AIY following vehicle (DMSO) or juglone treatment for 10min. Unlined *** and ###
1377 denotes statistical analysis compared to “wild type”. n = 30, 30, 29, 30, 30, 30 independent animals.
1378 **C** Quantification of average coelomocyte fluorescence of the indicated mutants expressing FLP-1::Venus
1379 fusion proteins in AIY following vehicle (DMSO) or juglone treatment for 10min. Unlined *** and ns denote
1380 statistical analysis compared to “wild type”. n = 24, 24, 25, 25, 30, 30 independent animals. Data are mean
1381 values ± s.e.m normalized to wild type controls. ns. not significant, *** and ### $P < 0.001$ by Brown-
1382 Forsythe and Welch ANOVA with Dunnett’s T3 multiple comparisons test.
1383

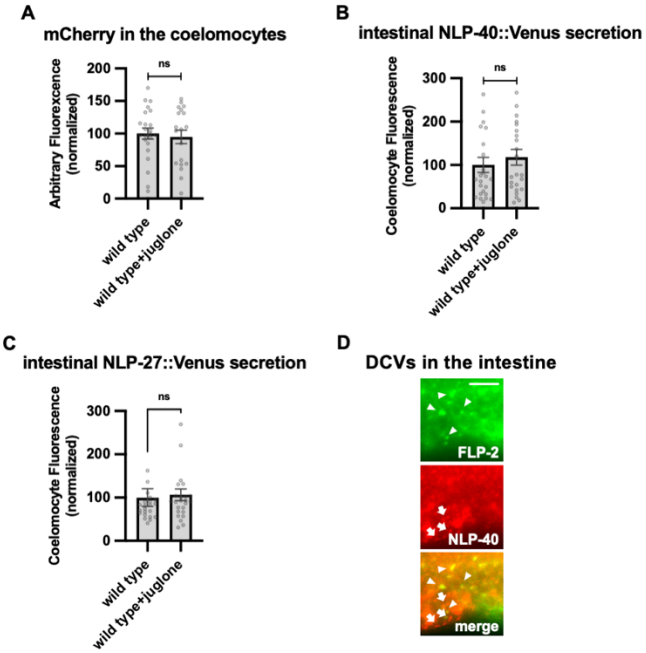

Supplementary Figure 2. Specificity of juglone on intestinal peptide secretion, and FLP-2 and NLP-40 localization in the intestine.

A Quantification of average coelomocyte fluorescence of the indicated mutants co-expressing FLP-2::Venus in the intestine (under the *ges-1* promoter) and mCherry in the coelomocytes (under the *ofm-1* promoter) following M9 or juglone treatment for 10min. n = 23, 19 independent animals.
B Quantification of average coelomocyte fluorescence of transgenic animals expressing NLP-40::Venus fusion proteins in the intestine following M9 or juglone exposure for 10min. n = 25, 24 independent animals.
C Quantification of average coelomocyte fluorescence of transgenic animals expressing NLP-27::Venus fusion proteins in the intestine following M9 or juglone exposure for 10min. n = 23, 25 independent animals.
D Representative images of fluorescence distribution in the posterior intestinal region of transgenic animals co-expressing FLP-2::Venus fusion proteins (marked by arrowheads) and NLP-40::mTur2 fusion proteins (marked by arrows). Scale bar: 5μM. Data are mean values ± s.e.m normalized to wild type controls. ns. not significant by Brown-Forsythe and Welch ANOVA with Dunnett's T3 multiple comparisons test.

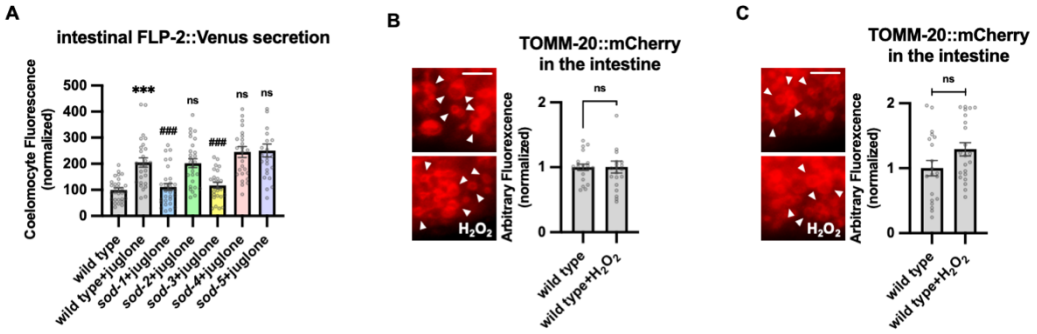

Supplementary Figure 3. SODs function in juglone induced FLP-2 release from the intestine and mitochondrial mCherry control.

A Quantification of average coelomocyte fluorescence of the indicated mutants expressing FLP-2::Venus fusion proteins in the intestine following M9 or juglone treatment for 10min. Unlined ***, ### and ns denote statistical analysis compared to “wild type+juglone”. n = 29, 27, 29, 27, 25, 26, 24 independent animals.

B and C Representative images and quantification of average fluorescence intensity of TOMM-20::mCherry proteins in transgenic animals co-expressing matrix-HyPer7 (B) or OMM-HyPer7 (C) following M9 or H_2O_2 treatment for 10min. (B) Scale bar: Scale bar: 5μM. n = 20, 20 independent animals. (C) Scale bar: Scale bar: 5μM. n = 20, 22 independent animals.

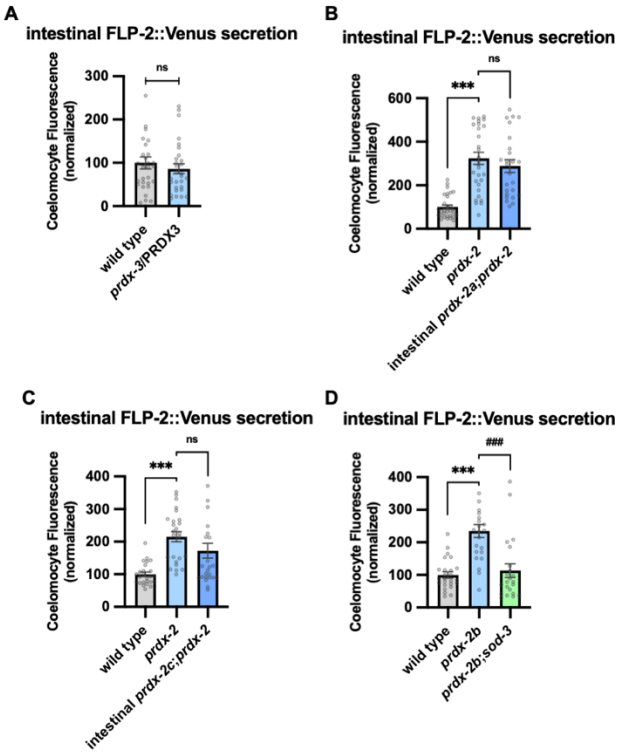

Supplementary Figure 4. PRDX-2 intestinal rescue and mediates SOD-3 dependent regulation of FLP-2 release.

A Quantification of average coelomocyte fluorescence of the indicated mutants expressing FLP-2::Venus fusion proteins in the intestine following M9 treatment for 10min. n = 30, 29 independent animals.

B Quantification of average coelomocyte fluorescence of the indicated mutants expressing FLP-2::Venus fusion proteins in the intestine following M9 treatment for 10min. Intestinal *prdx-2a* denotes expression of *prdx-2a* cDNA under the *ges-1* promoter. n = 30, 30, 25 independent animals.

C Quantification of average coelomocyte fluorescence of the indicated mutants expressing FLP-2::Venus fusion proteins in the intestine following M9 treatment for 10min. Intestinal *prdx-2c* denotes expression of *prdx-2c* cDNA under the *ges-1* promoter. n = 25, 25, 25 independent animals.

D Quantification of average coelomocyte fluorescence of the indicated mutants expressing FLP-2::Venus fusion proteins in the intestine following M9 treatment for 10min. n = 25, 23, 22 independent animals. Data are mean values ± s.e.m normalized to wild type controls. Data are mean values ± s.e.m normalized to wild type controls. ns. not significant, *** and ### $P < 0.001$ by Brown-Forsythe and Welch ANOVA with Dunnett's T3 multiple comparisons test.

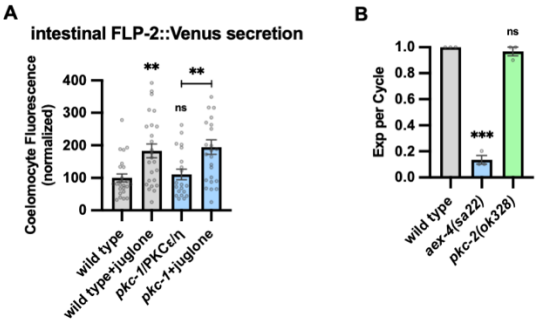

Supplementary Figure 5. Juglone promotes FLP-2 release in *pkc-1* mutants and expulsion analysis.
A Quantification of average coelomocyte fluorescence of the indicated mutants expressing FLP-2::Venus fusion proteins in the intestine following M9 or juglone treatment for 10min. Unlined ns and ** denote statistical analysis compared to “wild type”. n = 24, 25, 20, 25 independent animals.
B Quantification of the number of expulsions (Exp) per defecation cycle in adult animals of the indicated genotypes. n = 30, 30, 30, 30 in three independent animals. Data are mean values ± s.e.m normalized to wild type controls. ns. not significant, ** $P < 0.01$, *** $P < 0.001$ by Brown-Forsythe and Welch ANOVA with Dunnett’s T3 multiple comparisons test.

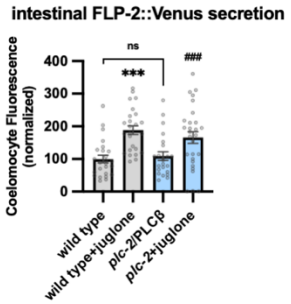

Supplementary Figure 6. Juglone promotes FLP-2 release in *plc-2* mutants.
Quantification of average coelomocyte fluorescence of the indicated mutants expressing FLP-2::Venus fusion proteins in the intestine following M9 or juglone treatment for 10min. Unlined *** denotes statistical analysis compared to “wild type”; unlined ### denotes statistical analysis compared to “*plc-2*/PLCβ”. n = 25, 25, 23, 28 independent animals. Data are mean values ± s.e.m normalized to wild type controls. ns. not significant, *** and ### $P < 0.001$ by Brown-Forsythe and Welch ANOVA with Dunnett’s T3 multiple comparisons test.

1446 **Table S1. Strains, transgenic lines and plasmids used in this study**

Strain	Genotype	Figures
N2	wild type Bristol strain	Fig. 1C, S5B
OJ6555	*flp-1(ok2811) IV*	Fig. 1C
OJ5490	*flp-2(ok3351) X*	Fig. 1C
OJ10228	*flp-1(ok2811);flp-2(ok3351)*	Fig. 1C
OJ7466	*aex-4(sa22) X*	Fig. S5B
VC127	*pkc-2(ok328) X*	Fig. S5B
OJ3614	*vjIs150[pJQ60(Pttx-3::flp-1::Venus)]*	Fig. 1A, 1B, 1D, S1B, S1C
OJ5616	*aex-5(sa23);vjIs150*	Fig. 1B
OJ5780	*vjEx1748[pJQ298(Prab-3::aex-5 cDNA)];aex-5(sa23);vjIs150*	Fig. 1B
OJ5785	*vjEx1753[pJQ299(Pges-1::aex-5 cDNA)];aex-5(sa23);vjIs150*	Fig. 1B
OJ6334	*vjEx1753;aex-5(sa23);flp-2(ok3351);vjIs150*	Fig. 1B
OJ5264	*flp-2(ok3351);vjIs150*	Fig. 1D
OJ8818	*vjEx2882[pJQ366(Prab-3::flp-2 gDNA)];flp-2(ok3351);vjIs150*	Fig. 1D
OJ8813	*vjEx2877[pJQ305(ges-1::flp-2 gDNA)];flp-2(ok3511);vjIs150*	Fig. 1D
OJ10229	*vjEx2877;vjIs150*	Fig. 1D
CL2166	*dvIs19[pAF15(Pgst-4::GFP::NLS)]*	Fig. 1E, 1F, 4F
OJ2547	*flp-1(ok2811);dvIs19*	Fig. 1E, 1F
OJ10230	*flp-2(ok3351);dvIs19*	Fig. 1E
OJ6544	*flp-1(ok2811);flp-2(ok3511);dvIs19*	Fig. 1E
OJ10231	*vjEx2877;dvIs19*	Fig. 1F
OJ10232	*vjEx2877;flp-1(ok2281);dvIs19*	Fig. 1F
OJ5888	*aex-1(sa9);vjIs150*	Fig. S1B
OJ5890	*aex-3(js815);vjIs150*	Fig. S1B
OJ5891	*aex-4(sa22);vIs150*	Fig. S1B
OJ5892	*aex-6(sa24);vjIs150*	Fig. S1B
OJ5615	*nlp-40(tm4085);vjIs150*	Fig. S1C
OJ5889	*aex-2(sa3);vjIs150*	Fig. S1C
OJ6405	*vjEx2035[pJQ305(Pges-1::flp-2 gDNA::Venus)]*	Fig. 2A, 2C, 2D, 2F, S2A, 3A, 3B, 3C, 3G, 3H, S3A, 4B, 4E, S4A, S4B, S4C, S4D, 5A, 5D, 5E, S5A, 6B, 6E, 6H, S6
OJ9469	*vjEx3069[pDY10(Pges-1::aex-5::mTur2)];vjEx2035*	Fig. 2B
OJ6409	*aex-4(sa22);vjEx2035*	Fig. 2C, 3G
OJ8345	*aex-6(sa24);vjEx2035*	Fig. 2C, 3G
OJ6641	*flp-1(ok2811);vjEx2035*	Fig. 2F
OJ1002	*vjIs40[pDS292(Pnlp-40::nlp-40::Venus)]*	Fig. S2B
OJ10237	*vjEx3263[pJQ370(Pges-1::nlp-27 gDNA::Venus)]*	Fig. S2C
OJ9567	*vjEx3062[pDY(Pges-1::nlp-40::mTur2)];vjEx2035*	Fig. S2D
OJ9797	*sod-1(tm783);vjEx2035*	Fig. 3A, 3H, S3A
OJ8588	*vjEx2814[pJQ419(Pges-1::sod-1b cDNA)];sod-1(tm783);vjEx2035*	Fig. 3A
OJ8341	*sod-3(tm760);vjEx0235*	Fig. 3B, 3H, S3A
OJ8933	*vjEx2910[pJQ389(Pges-1::sod-3 cDNA)];sod-3(tm760);vjEx2035*	Fig. 3B
OJ9106	*vjEx2973[pJQ408(Pges-1::sod-3(ΔMLS) cDNA)];sod-3(tm760);vjEx2035*	Fig. 3B
OJ10234	*sod-1(tm783);sod-3(tm760);vjEx2035*	Fig. 3C, 3H
OJ10243	*vjEx3266[pJQ420(Pges-1::sod-1b cDNA::GFP)]*	Fig. 3D
OJ9141	*vjEx2993[pJQ407(Pges-1::sod-3 cDNA::GFP)]*	Fig. 3E
OJ9144	*vjEx2996[pJQ409(Pges-1::sod-3(ΔMLS) cDNA::GFP)]*	Fig. 3F

OJ9230	*vjEx3020[pJQ383(Pges-1::MLS::HyPer7)]*	Fig. 3I, S3B, 5B, 6C, 6F
OJ9196	*vjEx3014[pJQ411(Pges-1::tomm-20::HyPer7)]*	Fig. 3I, S3C, 5C ,6D, 6G
OJ9281	*sod-1(tm783);vjEx3020*	Fig. 3I
OJ9259	*sod-3(tm760);vjEx3020*	Fig. 3I
OJ10244	*sod-1(tm783);sod-3(tm760);vjEx3020*	Fig. 3I
OJ9795	*sod-1(tm783);vjEx3014*	Fig. 3I
OJ9280	*sod-3(tm760);vjEx3014*	Fig. 3I
OJ10245	*sod-1(tm783);sod-3(tm760);vjEx3014*	Fig. 3I
OJ10238	*sod-2(ok1030);vjEx2035*	Fig. S3A
OJ10239	*sod-4(gk101);vjEx2035*	Fig. S3A
OJ10240	*sod-5(tm1146);vjEx2035*	Fig. S3A
OJ8991	*prdx-2(gk169);vjEx2035*	Fig. 4B, S3E, S3F ,4C, 5E
OJ10251	*prdx-2b(vj380);vjEx2035*	Fig. 4B, 4E, S4B
OJ8996	*vjEx2926[pJQ381(Pges-1::prdx-2b cDNA)];prdx-2(gk169);vjEx2035*	Fig. 4B
OJ9249	*trx-3(tm2820);vjEx2035*	Fig. 4B
OJ9496	*vjEx3091[pJQ422(Pges-1::trx-3 cDNA)];trx-3(tm2820);vjEx2035*	Fig. 4B
OJ10252	*trx-3(tm2820);sod-1(tm783);vjEx2035*	Fig. 4B
OJ10253	*trx-3(tm2820);sod-3(tm760);vjEx2035*	Fig. 4B
OJ9237	*prdx-2(gk169);vjEx3020*	Fig. 4C
OJ10247	*prdx-2b(vj380);vjEx3020*	Fig. 4C
OJ10249	*trx-3(tm2820);vjEx3020*	Fig. 4C
OJ10246	*prdx-2(gk169);vjEx3014*	Fig. 4D
OJ10248	*prdx-2b(vj380);vjEx3014*	Fig. 4D
OJ10250	*trx-3(tm2820);vjEx3014*	Fig. 4D
OJ10254	*prdx-2b(vj380);dvIs19*	Fig. 4F
OJ10255	*prdx-2b(vj380);flp-2(tm3351);dvIs19*	Fig. 4F
OJ10256	*prdx-3(gk529);vjEx2035*	Fig. S4A
OJ10258	*vjEx3268[pJQ380(Pges-1::prdx-2a cDNA)];prdx-2(gk169);vjEx2035*	Fig. S4B
OJ10260	*vjEx3270[pJQ399(Pges-1::prdx-2c cDNA)];prdx-2(gk169);vjEx2035*	Fig. S4C
OJ9250	*prdx-2b(vj380);sod-3(tm760);vjEx2035*	Fig. S4D
OJ9682	*pkc-2(ok328);vjEx2035*	Fig. 5A, 5D, 5E
OJ8682	*vjEx2828[pJQ376(Pges-1::pkc-2b cDNA)];pkc-2(ok328);vjEx2035*	Fig. 5A
OJ9657	*vjEx3131[pJQ446(Pges-1::pkc-2(K375R) cDNA)];pkc-2(ok328);vjEx2035*	Fig. 5A
OJ10279	*pkc-2(ok328);vjEx3020*	Fig. 5B
OJ10280	*pkc-2(ok328);vjEx3014*	Fig. 5B
OJ8939	*prdx-2(gk169);pkc-2(ok328);vjEx2035*	Fig. 5E
OJ10278	*pkc-1(nj3);vjEx2035*	Fig. S5A
OJ9863	*egl-8(sa47);vjEx2035*	Fig. 6B
OJ10281	*egl-8(sa47);vjEx3020*	Fig. 6C
OJ10282	*egl-8(sa47);vjEx3014*	Fig. 6D
OJ10263	*dgk-2(gk124);vjEx2035*	Fig. 6E, 6H
OJ10264	*vjEx327[pJQ460(Pges-1::dgk-2a cDNA)];dgk-2(gk124);vjEx2035*	Fig. 6E
OJ10266	*dgk-2(gk124);pkc-2(ok328);vjEx2035*	Fig. 6E
OJ10283	*dgk-2(gk124);vjEx3020*	Fig. 6F
OJ10284	*dgk-2(gk124);vjEx3014*	Fig. 6G
OJ9809	*plc-2(ok1761);vjEx2035*	Fig. S6

1447